Studies on the $Ne^{20}(d,p\gamma)Ne^{21}$ Reaction*†

A. J. HOWARD AND D. A. BROMLEY
Yale University, New Haven, Connecticut

AND

E. K. WARBURTON
Brookhaven National Laboratory, Upton, New York

(Received 20 August 1964)

The Ne^{21} states below an excitation energy of 5 MeV have been investigated through study of the Ne^{20}-$(d,p\gamma)Ne^{21}$ reaction with deuteron energies in the range below 3 MeV. Precise de-excitation branching ratios have been determined for the 1.75-, 2.80-, 3.67-, and 4.73-MeV Ne^{21} states; the most prominent gamma de-excitation mode for all but one of the eleven excited states of Ne^{21} up to an excitation energy of 4.73 MeV have been established. The lowest excitation in Ne^{21} was determined to be 353 ± 1.5 keV, and an unambiguous J^π assignment of $\frac{5}{2}^+$ and a mean lifetime of $<3\times10^{-10}$ sec were also established; the $E2$-to-$M1$ amplitude ratio for this state de-excitation was measured to be $-0.02\leq\delta\leq+0.03$. A J^π assignment of $\frac{7}{2}^+$ is strongly suggested for the 1.75-MeV Ne^{21} second excited state, and both a significant $(7\pm1\%)$ $E2$ de-excitation radiation branch to the $\frac{3}{2}^+$ ground state and $E2$ admixture in the cascade transition to the $\frac{5}{2}^+$ first excited state have been established. A J^π assignment of $\frac{1}{2}^+$ for the 2.80-MeV Ne^{21} state is confirmed, and the existence of a $10\pm1\%$ $E2$ cascade de-excitation to the $\frac{5}{2}^+$ 0.353-MeV state has been established. Further data indicates that $J\geq\frac{5}{2}$ and $\frac{3}{2}$ for the 2.87- and 3.67-MeV Ne^{21} states, respectively, and strongly imply that the 3.74- and 3.57-MeV states in Ne^{21} and Na^{21}, respectively, are mirror analog $\frac{5}{2}^+$ states. An unambiguous J^π assignment of $\frac{3}{2}^-$ is evidenced for the 4.73-MeV Ne^{21} state. Available evidence supports the general validity of a strong-coupling collective model interpretation of the Na^{21} structure.

I. INTRODUCTION

THE research to be reported herein, on which preliminary reports have already been published,[1,2] concerns the study of the de-excitation gamma radiations originating from excited states in Ne^{21} formed in the $Ne^{20}(d,p)Ne^{21}$ reaction. Successes in the application of a strong coupling collective-model description to nuclei in the region[3,4] of mass 25 have prompted further studies on nuclei in this mass region of the *sd* shell. Evidence that the collective-model approach[5] might adequately describe the level structure of the Na^{23} nucleus[6] suggests that a similar description should be informative in the mass-21 system; the odd-nucleon count, hereafter denoted by ζ, is 11 for O^{19}, Ne^{21}, Na^{21}, and Na^{23}. A preliminary application of the Nilsson strong-coupling model elucidated by Litherland *et al.*[3] has been made to the Ne^{21} level structure,[7] and the static properties of the Ne^{21} system have also been recently interpreted within a collective-model framework.[8] More generally, the Chi-Davidson asymmetric-core rotator model has been elaborated for nuclei throughout the $2s$-$1d$ nuclear shell,[4] with specific formalisms generated to describe both the static and dynamic properties of the Ne^{21}, Na^{21}, and Na^{23} nuclear systems; insufficient data are available as yet to permit establishment of the model parameters in the case of O^{19}.

A literature survey reveals that although extensive studies of the excitation energies, via particle spectra measurements, have been previously carried out,[9–14] no detailed studies on the de-excitation gamma radiations have been reported for the Ne^{21} system. Burrows *et al.*[12] measured the excitation energies and angular distributions (over a restricted forward angle range) of nine proton groups corresponding to formation of Ne^{21} nuclear states via the (d,p) reaction; gaseous neon of natural isotopic abundance (90.8% Ne^{20}, 0.26% Ne^{21}, 8.9% Ne^{22}) was employed for the target material, the incident deuterons were of 8.5-MeV energy, and a magnetic momentum analysis of the outgoing protons was carried out. Freeman[13] established excitation energies of 27 excited states in the Ne^{21} system up to

* Work supported in part by the U. S. Atomic Energy Commission.

† Part of the research reported herein was submitted by A. J. Howard in partial fulfillment of the requirements for the Ph.D. degree at Yale University, 1963.

[1] A. J. Howard, D. A. Bromley, and E. K. Warburton, Bull. Am. Phys. Soc. **8**, 47 (1963).

[2] A. J. Howard, Doctoral dissertation, Yale University, 1963 (unpublished).

[3] A. E. Litherland, H. McManus, E. B. Paul, D. A. Bromley, and H. E. Gove, Can. J. Phys. **36**, 378 (1958).

[4] B. E. Chi and J. P. Davidson, Phys. Rev. **131**, 366 (1963).

[5] G. Rakavy, Nucl. Phys. **4**, 375 (1957).

[6] E. B. Paul and J. H. Montague, Nucl. Phys. **8**, 61 (1958).

[7] J. M. Freeman, in *Proceedings of the International Conference on Nuclear Structure, 1960*, edited by D. A. Bromley and E. Vogt (University of Toronto Press, Toronto, 1960), p. 447.

[8] R. M. Dreizler, Phys. Rev. **132**, 1166 (1963).

[9] A. Zucker and W. W. Watson, Phys. Rev. **78**, 14 (1950).

[10] R. Middleton and C. T. Tai, Proc. Phys. Soc. (London) **A65**, 752 (1952).

[11] K. Ahnlund, Arkiv Fysik **9**, 39 (1955).

[12] H. B. Burrows, T. S. Green, S. Hinds, and R. Middleton, Proc. Phys. Soc. (London) **A69**, 310 (1956).

[13] J. M. Freeman, Phys. Rev. **120**, 1436 (1960).

[14] S. Hinds and R. Middleton, Proc. Phys. Soc. (London) **74**, 779 (1959).

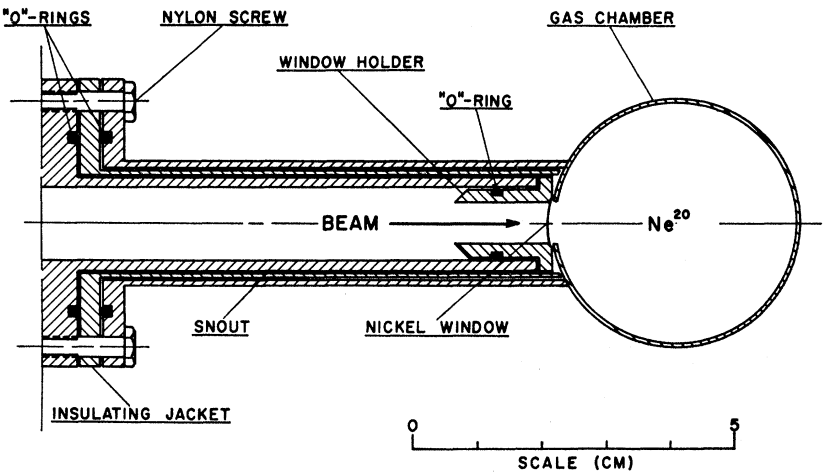

FIG. 1. Schematic diagram of the gas-target chamber.

$E_x = 6.75$ MeV, to within ± 0.01 MeV in all cases: Neon gas of varied isotopic constituency formed the targets, deuteron beams in the energy range 4.75–7.50 MeV were employed, and the proton groups were analyzed with a broad-range magnetic spectrograph at $\theta = 90°$ only. Hinds and Middleton[14] carried out an investigation of the Ne^{21} level structure via the $F^{19}(He^3,p)Ne^{21}$ reaction: A thin solid calcium fluoride target was used, the He^3 beam energy was 5.87 MeV, and a broad-range magnetic spectrograph analyzed the proton groups. Their results established the excitation energies of 67 states in the Ne^{21} nucleus up to $E_x = 9.34$ MeV, to within ± 0.01 MeV in all cases. In the region of comparison for the determinations by Freeman and by Hinds and Middleton, the level positions are in excellent accord, being within the assigned limits of error in all cases.

In contrast with the extensive charged particle studies described above, only limited observations on the de-excitation gamma radiations in the Ne^{21} system have been recorded.[15–18] Gorodetsky *et al.*[15] investigated the $Ne^{20}(d,p\gamma)Ne^{21}$ reaction: Neon gas of natural isotopic purity formed the target, the energy of the incident beam was in the vicinity of 1 MeV, and proton-gamma coincidence techniques were applied. The de-excitation gamma rays from the first three excited states of Ne^{21} were observed, and the correct identification of three transitions was made. Khabakhpashev and Tsenter[16] studied the gamma-ray transitions originating from the second excited state in the Ne^{21} system, which they formed by the $O^{18}(\alpha,n)Ne^{21}$ reaction in an intimate Po-O^{18} mixture. A gamma-gamma angular correlation experiment was performed on the cascade gamma rays involving the intermediate first excited state of Ne^{21}, and a lifetime measurement for the first excited state by gamma-gamma coincidence techniques indicated a mean lifetime of less than 10^{-10} sec.

Studies on the $F^{19}(He^3,p\gamma)Ne^{21}$ reaction have recently been reported by Pelte *et al.*[17]: A J^π assignment of $\frac{7}{2}^+$ for the 1.75-MeV Ne^{21} state was indicated by proton-gamma angular correlation measurements, as was a $J = \frac{1}{2}$ or $\frac{3}{2}$ limitation for the 3.67-MeV state: gamma-ray branching ratios were obtained for the above states and also for the 2.80- and 2.87-MeV states. An investigation of the states below an excitation energy of 3 MeV in Ne^{21} has also been reported by Bent *et al.*,[18] who have utilized the $Be^9(O^{16},\alpha\gamma)Ne^{21}$ reaction to obtain lifetimes and preliminary branching ratio data for these states.

This survey suggested that investigation of the de-excitation gamma radiations in the Ne^{21} nuclear system could provide data crucial for a detailed examination of the validity of a strong-coupling collective-model interpretation for the Ne^{21} member of the $\zeta = 11$ system. The fact that (d,p) reactions characteristically proceed with high yield even at low energies was one of several factors which entered into the choice of the $Ne^{20}(d,p)Ne^{21}$ reaction as the method of population for the states under scrutiny: the large, positive ground-state Q value for this reaction, $Q = +4.53$ MeV, and the relatively low Q values associated with competing reactions, such as the (d,α) and (d,n), for which the respective ground-state Q values are $+2.78$ and $+0.22$ MeV, respectively, greatly reduced experimental difficulties and the importance of these competing reactions. The states in Ne^{21} are bound up to an excitation energy of 6.75 MeV, and it was thus energetically possible to form all bound states in the Ne^{21} system with the deuteron energies ($E_d \leq 3$ MeV) available for this investigation. Finally, monoisotopic Ne^{20} gas was available for target use; ambiguities which would otherwise be present concern-

[15] S. Gorodetsky, Th. Muller, and M. Port, J. Phys. Radium **17**, 549 (1956).

[16] A. G. Khabakhpashev and É. M. Tsenter, Izv. Akad. Nauk SSSR Ser. Fiz. **23**, 883 (1959); Zh. Eksperim. i Teor. Fiz. **37**, 991 (1959) [English transl.: Soviet Phys.—JETP **10**, 705 (1960)].

[17] D. Pelte, B. Povh, and W. Scholz, Nucl. Phys. **55**, 322 (1964).

[18] R. D. Bent, J. E. Evans, G. C. Morrison, and I. J. Van Heerden, in *Proceedings of the Third Conference on Reactions Between Complex Nuclei*, edited by A. Ghiorso, R. M. Diamond, and H. E. Conzett (University of California Press, Berkley and Los Angeles, 1963), p. 417.

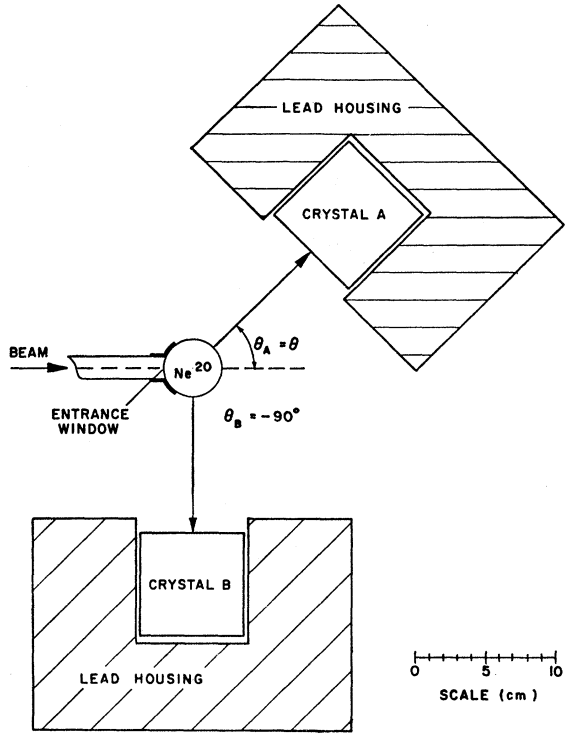

FIG. 2. Schematic diagram of gamma-gamma angular correlation geometry.

ing gamma radiations arising from nuclear reactions with the other neon isotopes were thus eliminated.

II. APPARATUS

Deuteron beams used herein were obtained from the 3-MeV Brookhaven National Laboratory Van de Graaff accelerator. The targets were gaseous Ne^{20} of isotopic purity 99.99%; an upper limit of 0.1% nitrogen impurity was ascertained by mass spectrometer analyses, and no other contaminants ($\leq$0.001%) were detected in the target gas. The separated Ne^{20} gas samples were produced via a thermal diffusion column technique by the Yale isotope separation group.[19]

Figure 1 is a schematic illustration of the gas-target assembly used in these measurements. It consisted of a 3-cm-diam by 4-cm-long cylindrical shell mounted with its axis of rotation perpendicular to the horizontal beam vector. The brass shell was 0.05 cm in thickness and was internally lined with 0.01-cm-thick tantalum foil. The top of the target chamber was removable and was sealed to the cylindrical chamber body by an O-ring seal assembly. This allowed the liner of the chamber to to be removed periodically for removal of contaminants, oxides, etc., which were formed during prolonged bombardment and also permitted the insertion of solid-state detectors into the target area.

[19] A. J. Howard and W. W. Watson, J. Chem. Phys. 40, 1409 (1964).

The deuteron beam entered the target chamber through a 0.625-cm-diam by 0.00025-cm-thick nickel retaining window. The window assembly fitted into a 8.5-cm-long cylindrical brass snout, whose axis of rotation was parallel to the beam vector; the target volume was insulated from the snout window component by a Plexiglas jacket. In this manner the target volume was electrically isolated and the beam currents were measured directly from it. In order to minimize the rate of contaminant deposit on the entrance window of the target chamber, the entire target assembly was secured to an adjacent liquid-nitrogen transmission cold trap.

A three-element collimation system comprising circular tantalum apertures limited the maximum beam aperture and angular divergence to 0.3 cm and $\sim$1°, respectively.

The magnetically analyzed beam from the Van de Graaff accelerator was regulated by two servo-regulation slits placed 1 cm behind the first collimator disk to within $\pm$5 keV.

A Ne^{20} gas handling system was used to evacuate the target chamber to 1 μ of mercury pressure before introduction of the Ne^{20} gas and to maintain the target gas pressure to within 1% during the experimental investigations.

Preliminary investigation of the gamma rays discussed herein was made with two 5-in.-diam by 4-in.-long NaI(Tl) spectrometers having uncollimated energy resolutions of 13 and 16% for the 0.66 Cs^{137} gamma-ray, respectively (source distance=16 cm). Later studies were carried out with two 3-in.-diam by 3-in.-long NaI(Tl) crystals, with corresponding energy resolutions of 7.5 and 8.0%. A 1.5-in.-diam by 3-in.-long NaI(Tl) crystal was employed as the center crystal in a three-

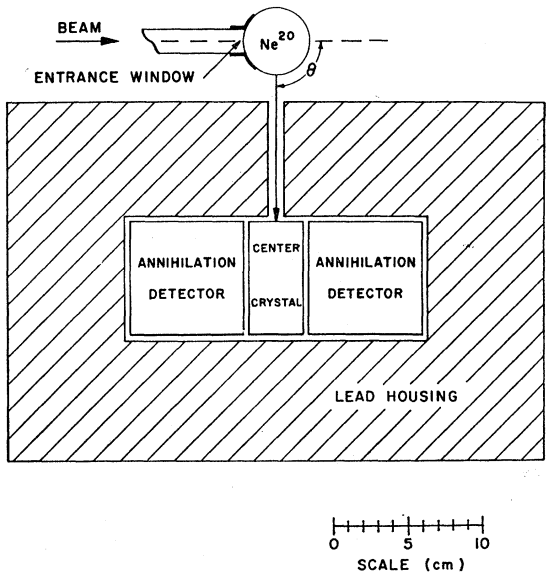

FIG. 3. Schematic diagram of the three-crystal pair spectrometer.

crystal pair-spectrometer configuration; this was determined to have an energy resolution of 7.0% for the Co^{60}, 1.13-MeV line from a source 10 cm from the crystal face.

Particle detection was carried out with a 0.5-cm square Au-silicon surface barrier detector with a depletion layer of $\sim 200\,\mu$ thickness at 200 V applied bias and an energy resolution of 1.2% for 4.8-MeV alpha particles. This detector, as well as the gamma-ray spectrometers, was used in conjunction with standard electronic pulse routing systems.[20]

III. PROCEDURES

A. Gamma-Ray Angular Distribution Studies

Measurements were performed with both the 5-in. by 4-in. and 3-in. by 3-in. crystals mounted on a simple angular correlation table; the front face of the crystal was located 16 cm and 12 cm from the target center in the respective cases. The symmetry axis of the crystal (crystal A) was coplanar with the beam vector, the intersection point being the target center. A second crystal (crystal B) was similarly located at a fixed angle of 90° to the beam vector. This arrangement allowed crystal A to be rotated about the target center in the horizontal plane at a fixed target-to-detector distance over an angle range of 0–120° with respect to the beam vector. The lead shielding arrangement is shown in Fig. 2. Direct spectra obtained from both crystals A and B were recorded simultaneously in two 400-channel analyzers; the spectrum associated with crystal A was used to determine the angular distribution of the gamma radiations with respect to the beam vector, whereas that obtained from the crystal B served as a monitor during sequential angular distribution measurements. The majority of these measurements were recorded in sets taken at staggered 15° intervals from $\theta = 0$ to 90°, a repetition being made at the extreme angles as a second determination of the anisotropy associated with the gamma radiations under surveillance.

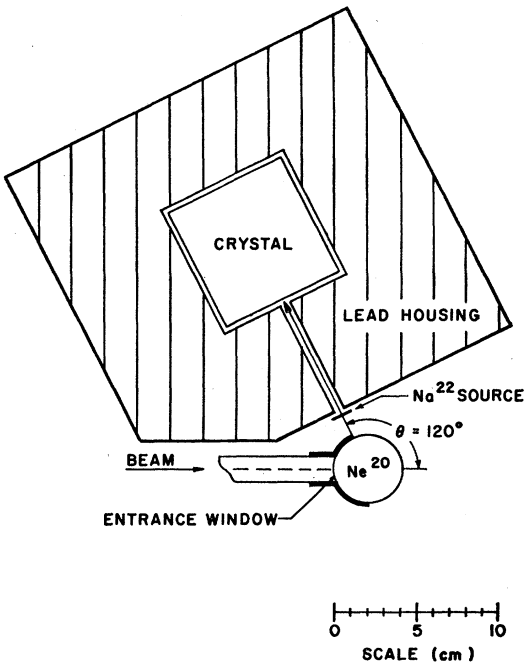

FIG. 4. Schematic diagram of the Doppler-shift geometry.

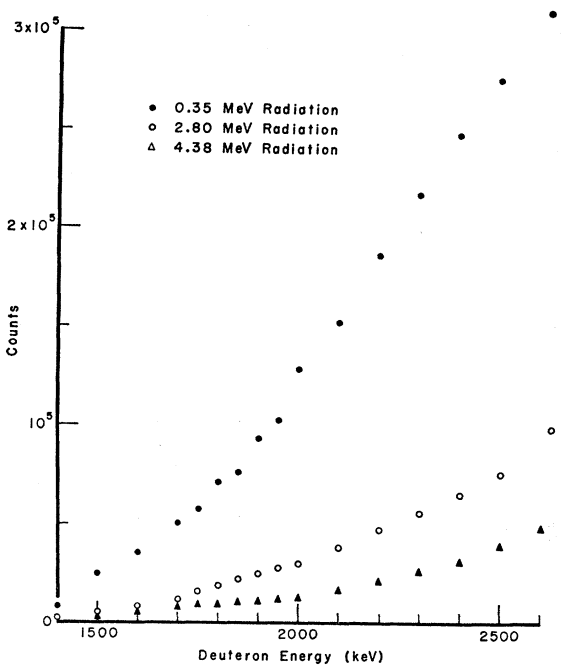

FIG. 5. $Ne^{20}(d,p\gamma)Ne^{21}$ gamma-ray yield measurements.

B. Proton-Gamma Coincidence Studies

The solid-state detector was located in the target volume with its normal vector at right angles to the beam vector and in the horizontal plane defined by these vectors. The detector was approximately 1 cm distant from the target center; the gamma-ray spectrometer was located with its front face 4 cm from the target center. Voltage intervals corresponding to the selected regions of the proton spectra were used to establish the time coincidence conditions, the gamma-ray spectra being recorded at angles of 0 and 90° with respect to the incident beam.

C. Gamma-Gamma Coincidence and Angular Correlation Studies

The gamma-gamma coincidence studies were made with both NaI(Tl) crystals located with their symmetry axes normal to the beam vector. In order to maximize

[20] R. L. Chase *Gamma Spectrometry* (McGraw-Hill Publishing Company, Inc., New York, 1962).

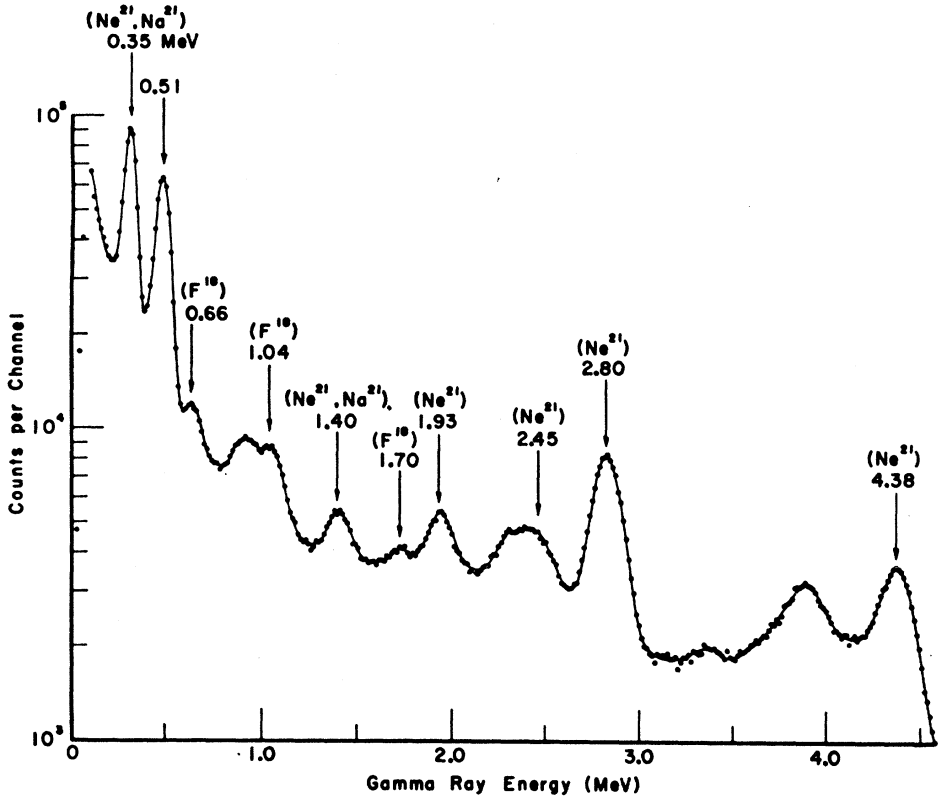

FIG. 6. $Ne^{20}+d$ direct gamma-ray spectrum obtained with 5-in.×4-in. sodium iodide crystal located at $\theta=90°$; the beam current was 0.2 nA, the integrated current was 15 nC, the deuteron beam energy was 2.90 MeV, and the target gas pressure was 60 cm of mercury absolute.

the real-to-random coincidence ratio, the front faces of both crystals were placed as close to the target as possible, namely 3.25 cm.

A cable curve was obtained for a Co^{60} test source by varying both the attenuation of the input signals to the fast coincidence circuit and the delays in the discriminator circuits; attenuations and delays were then selected so that the fast coincidence-circuitry efficiency remained constant for input pulses corresponding to gamma radiations in the 0.3–5.0-MeV energy range, the time resolution used being in the vicinity of 50 nsec.

The geometry for the gamma-gamma angular correlation studies was identical to that employed for the angular distribution measurements (Fig. 2). For these measurements, the gamma-ray spectrum of the variable position crystal A taken in time coincidence with the selected region of the gamma-ray spectrum of crystal B was recorded in one multichannel analyzer. The second analyzer served to monitor the gains of the A and B circuits, enabling correction for circuitry drifts of the entire detection system outside the multichannel analyzers to be made.

D. Three-Crystal Pair-Spectrometer Studies

A three-crystal annihilation pair spectrometer[21] was used for further angular distribution studies on the high-energy region of the $Ne^{20}+d$ gamma radiation spectrum (Fig. 3). The front face of the 1.5-in.-diam by 3-in.-long NaI(Tl) crystal was mounted at a distance of 12 cm from the target center, while the 3-in.-diam by 3-in.-long crystals were used as the side detectors. The entire assembly was encased in a lead shield, incorporating a 1-cm collimator aperture on the center crystal. Time resolutions of 25 nsec were used typically in these studies.

E. Doppler-Shift Studies

Doppler-shift measurements were carried out on the 0.35-MeV gamma ray in the $Ne^{20}+d$ spectrum, which corresponds to the de-excitation radiation from the first excited state in Ne^{21}. For these measurements, the geometry described for the angular distribution and correlation studies was employed. In order to optimize the geometry for this determination, however, the 3-in.-diam by 3-in.-long detector was encased in a 3-in.-thick lead housing with a 0.5-cm central collimating aperture (Fig. 4). An annihilation radiation reference source (Na^{22}) was positioned over the aperture on the external face of the shield. Twelve spectra were taken with angle settings $\theta=0$ and 120° being made alternately. The Doppler shift in the 0.35-MeV radiation from the (moving) Ne^{21} product nuclei was measured relative to the 0.511-MeV radiation from the

[21] D. A. Alburger and B. J. Toppel, Phys. Rev. **100**, 1357 (1955).

stationary source, the two gamma radiations being simultaneously recorded in the spectrum.

IV. PRELIMINARY INVESTIGATIONS

The gamma-ray spectrometers were calibrated using a variety of standard radioactive sources, with due care being taken to match counting rates to correct at least in first order for any rate-dependent gain shifts in the system.

A. Direct Spectra

Direct gamma-radiation spectra for the $Ne^{20}(d,p\gamma)$-Ne^{21} reaction were obtained in a 5-in.-diam by 4-in.-long sodium iodide crystal located at $\theta=90°$ in the angular distribution geometry (Fig. 2). Deuteron bombardment energies in the 0.9–2.9-MeV range were employed, spectra being obtained at 0.10-MeV intervals within this range. The Ne^{20} gas was at a pressure of 60 cm of mercury absolute, and the integrated current for each spectrum was 15 nC. The yield curves for the three most prominent gamma-ray transitions in the Ne^{21} nuclear system indicated that no gross resonance structure was evident in the $Ne^{20}(d,p\gamma)Ne^{21}$ reaction, the yields increasing monotonically as the deuteron energy approached the Coulomb barrier energy (Fig. 5).

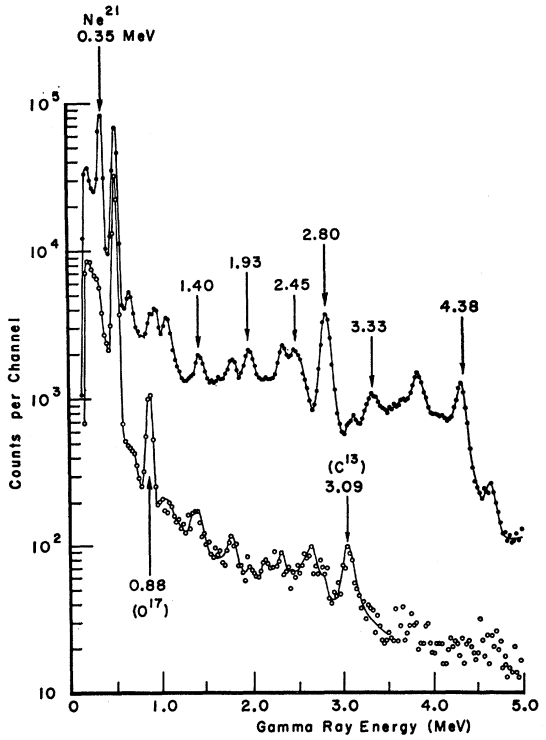

FIG. 7. $Ne^{20}+d$ direct gamma ray spectrum obtained with 3″×3″ sodium iodide crystal located at $\theta=0°$; the beam current was 0.2 nA, the integrated current was 50 nC, and the deuteron beam energy was 2.90 MeV. The target-gas pressure was 60 cm of mercury absolute for the foreground spectrum (closed circles) and 0.001 cm of mercury absolute for the background spectrum (open circles).

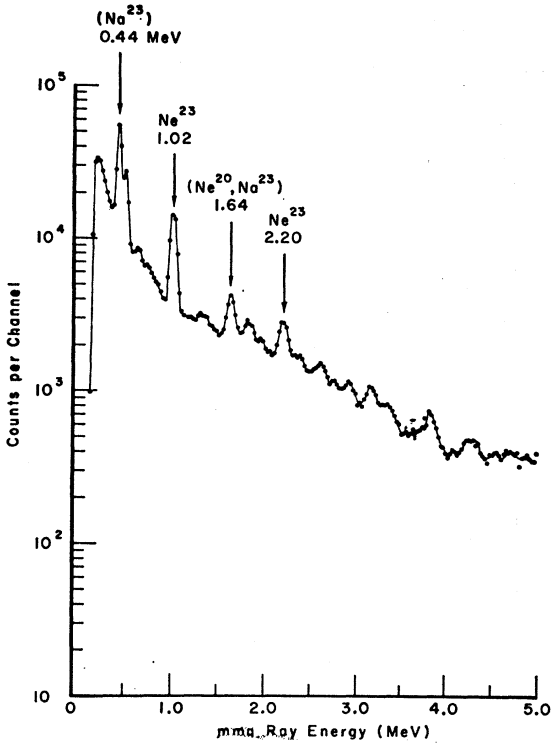

FIG. 8. $Ne^{22}+d$ direct gamma-ray spectrum obtained under conditions similar to those for the foreground spectrum in Fig. 7.

The direct spectra of the gamma radiations from the $Ne^{20}+d$ reaction obtained in both the 5-in.-diam by 4-in.-long, and 3-in.-diam by 3-in.-long sodium iodide crystal spectrometers are presented for comparison (Figs. 6 and 7, respectively). Also shown in Fig. 7 is a direct spectrum obtained under identical conditions but with the target volume evacuated to 0.001 cm of mercury absolute pressure. The identified peaks in the background spectrum were the result of (d,p) reactions on C^{12} and O^{16}, corresponding to the formation of the 3.09-MeV C^{13} and 0.875-MeV O^{17} excited nuclear states. The contaminant gamma radiations arising from deuteron-induced reactions in the target chamber were found to be almost negligible in comparison with the legitimate $Ne^{20}+d$ spectrum. It should be noted that these spectra were obtained at the conclusion of a 96-h run using the same nickel window; the carbonaceous contaminant build up on the window was by no means minimal for these spectra.

Analysis of the $Ne^{20}+d$ gamma-ray spectrum indicated the presence of prominent photopeaks of energies 0.35, 0.51, 0.94, 1.04, 1.40, 1.93, 2.80, and 4.38 MeV. Comparatively less intense gamma-ray photopeaks were identified at energies 0.66, 1.70, 2.45, 3.33, 3.52, and 4.74 MeV. The error in the assigned energy was less than 1% in all cases. The 0.35-, 1.40-, and 2.80-MeV transitions have previously been reported,[15–18] and subsequent measurements reported herein confirmed

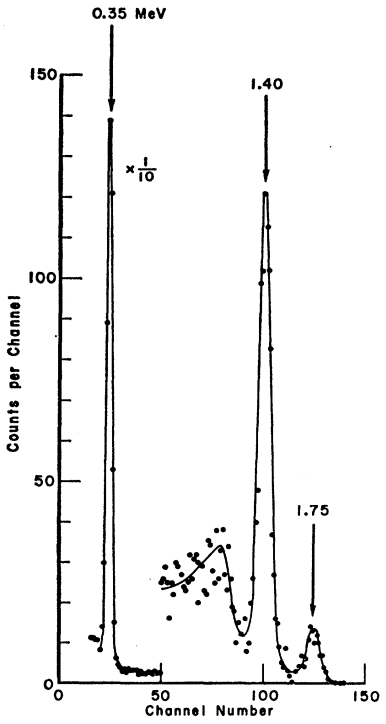

FIG. 9. Gamma radiation observed at $\theta=90°$ in time coincidence with the proton group populating the 1.75-MeV Ne^{21} state. $E_d=2.20$ MeV.

their previous transition assignments in the Ne^{21} nuclear system. The possibility that any of the weaker transitions noted above might have originated from deuteron-induced reactions on the 0.01% Ne^{22} present in the gas was eliminated by observations made using a 99.99% Ne^{22} gas target; the spectrum displayed in Fig. 8 was obtained under similar experimental conditions to those discussed above.

B. Proton-Gamma Coincidence Studies

Upon consideration of the energy-level spacing of the excited states in Ne^{21} (Fig. 26), five regions of the proton spectrum observed via the solid-state detector under conditions analogous to those described above were selected for time-coincidence measurements. These regions corresponded to the proton groups populating the following states in Ne^{21}: (1) the ground state, (2) the 0.353-MeV state, (3) the 1.75-MeV state, (4) the 2.80- and 2.87-MeV states, and (5) the 3.67-, 3.74-, and 3.89-MeV states. Q-value considerations indicated that region (5) was the only region in which alpha particles corresponding to the formation of excited states in F^{18} via the (d,α) reaction were to be expected. Lower energy proton groups were occluded by elastically scattered deuterons, and no attempt was made to degrade either the alpha particles or these deuterons. In all cases, the particle gates were about 300 keV wide, the gamma-ray spectrometer being used to distinguish the radiations originating from states whose particle groups were contained within the same particle gate region.

The gamma-ray spectrum observed in time coincidence with particle region (1) indicated that this region contained only the proton group corresponding to the formation of the Ne^{21} ground state; no gamma radiations were detected. A similar measurement involving the region (2) of the particle spectrum demonstrated that this region contained only the proton group corresponding to the formation of the 0.353-MeV state in Ne^{21}; only the 0.353-MeV radiation was detected. As illustrated in Fig. 9, region (3) contained the proton group corresponding to the formation of the 1.75-MeV Ne^{21} state; when the gamma-ray spectra observed at angles of 0 and 90° with respect to the deuteron beam were corrected for efficiencies and sum peaking, it was determined that $7\pm1\%$ of the de-excitation radiations from the 1.75-MeV Ne^{21} state proceed to the ground state, the remaining $93\pm1\%$ cascade to the 0.353-MeV state. The measurements just described were all taken with $E_d=2.20$ MeV.

Region (4) was the first particle region in which more than one group of particles were anticipated to be

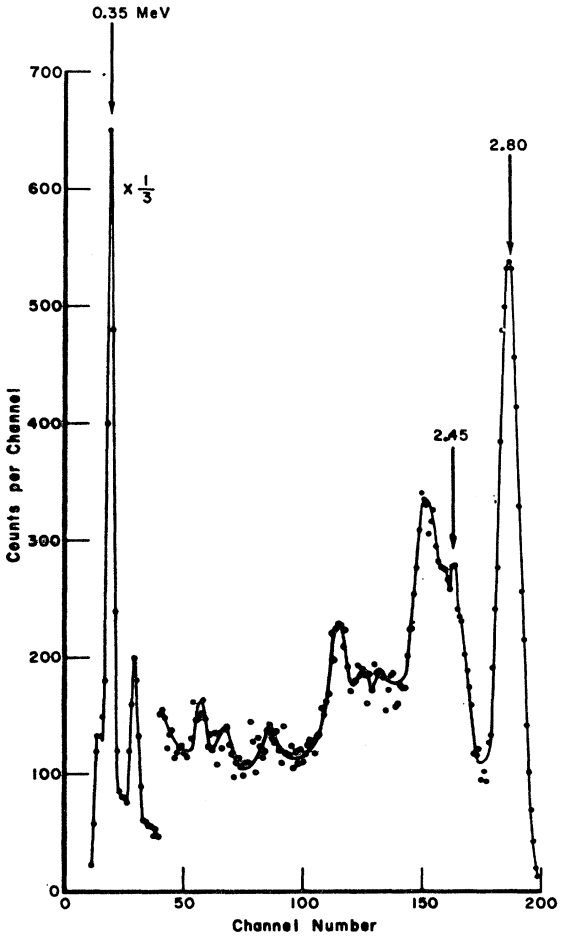

FIG. 10. Gamma radiation observed at $\theta=90°$ in time coincidence with the proton groups populating the 2.80- and 2.87-MeV Ne^{21} states. $E_d=2.20$ MeV.

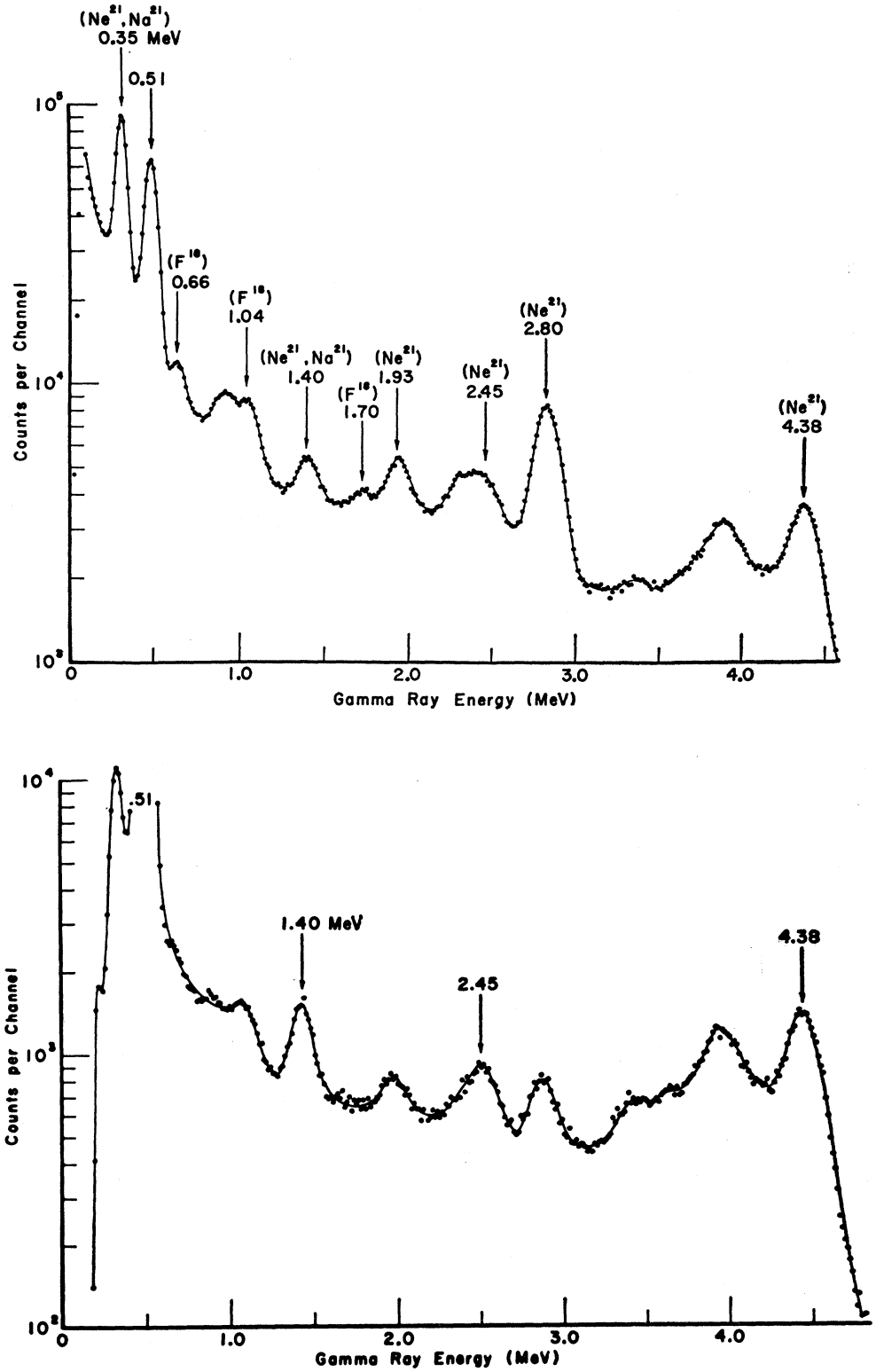

FIG. 11. $Ne^{20}+d$ gamma-ray spectra observed in 5-in.× 4-in. sodium iodide crystal. Upper spectrum is direct spectrum observed in crystal A (see Fig. 2) at $\theta_A=0°$. Lower spectrum is obtained in crystal A when gated by 0.35-MeV radiation observed in crystal B at $\theta_B=-90°$. $E_d=2.90$ MeV.

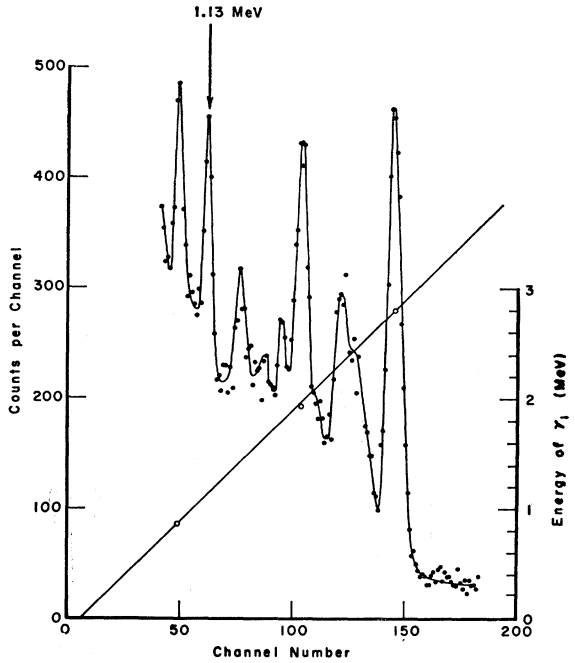

FIG. 12. $Ne^{20}+d$ spectrum observed via 3-in.×3-in. sodium iodide crystal in time coincidence with 1.40-MeV radiation; $\theta_A=90°$, $\theta_B=-90°$. The 1.13-MeV radiation was determined to be in time coincidence with the 1.40-MeV gamma ray, and the other peaks observed originated from time coincidence with the Compton tails associated with higher energy cascade gamma radiations. $E_d=2.90$ MeV.

contained, namely, those corresponding to the formation of the close lying 2.80- and 2.87-MeV Ne^{21} states. The gamma-ray spectra observed in time coincidence with the particles in this region indicated the presence of intense gamma-ray photopeaks of energies 2.80 and 0.35 MeV for $E_d=2.20$ MeV. Also detected was a weak photopeak observed at an energy of 2.45 MeV; spectra taken at angles of 0 and 90° with respect to the deuteron beam appeared isotropic within the limits of the experimental uncertainty, 4%. Analysis of the spectrum shown in Fig. 10 established that the 2.80-MeV Ne^{21} state decays $90\pm1\%$ to the ground state and $10\pm1\%$ to the 0.353-MeV Ne^{21} state. The previously reported[15] transition from the 2.80-MeV Ne^{21} state to the 1.75-MeV state was not observed, the erroneous assignment being traced to the presence of 10% Ne^{22} in the target gas employed for that study (see also Fig. 8). No radiations corresponding to de-excitation transitions originating from the 2.87-MeV Ne^{21} state were detected in these measurements, and it was concluded that the relative population of the 2.87-MeV state in this reaction at $E_d=2.20$ MeV was less than 0.1 of that of the 2.80-MeV state.

The measurement described in the preceding paragraph was also repeated with a higher value for the energy of the incident deuteron, $E_d=2.90$ MeV. When these spectra were compared with those taken with the lower bombardment energy, it was determined that the weak peaks in the vicinity of 1.10 and 1.40 MeV appeared more prominent in the former spectra. It was concluded that the 2.87-MeV Ne^{21} state de-excites in part by a cascade transition to the 1.75-MeV state.

The weak particle groups included in region (5) of the particle spectrum were found to be predominantly due to the (d,α) reaction; the particle–gamma-ray time-coincidence measurement did not establish the de-excitation properties for the 3.67-, 3.74-, or 3.89-MeV states.

C. Gamma-Gamma Coincidence Studies

Seven regions of the $Ne^{20}+d$ gamma-ray spectrum (Figs. 6 and 7) were selected for time-coincidence measurements; these regions included the gamma-ray photopeaks observed at 0.353, 1.04, 1.40, 1.70, 1.93, 2.80, and 4.38 MeV in the direct spectrum. Analyses of the direct spectrum indicated that the respective gamma-ray photopeak contributions were approximately 80, 55, 30, 10, 35, 80, and 98% of the total spectrum contained in the coincidence gating windows. The real-to-random ratios for these coincidence measurements were computed to be in the range 10:1 to 30:1, and so contamination of the coincidence spectra in most cases was primarily due to legitimate coincidences with the background spectrum contained in the gating windows.

The spectrum observed in time coincidence with the 0.353-MeV radiation included strongly coincident gamma radiations of energies 1.40, 2.45, 3.33, and 4.38 MeV. Also evidenced in weak coincidence were the gamma rays of energies 0.88, 1.12, 1.93, 3.52, and 4.17 MeV (Figs. 11 and 14). Of the gamma rays in the latter group, only the 1.93-MeV transition is prominently found in the direct spectra (Figs. 6 and 7).

With the coincidence gate positioned on the 1.64-MeV radiation, only the 0.66-MeV radiation was identified as being in time coincidence. As determined also from the measurements discussed in the preceding subsection, no evidence for the previously reported[15] transition from the 2.80-MeV to the 1.75-MeV Ne^{21} nuclear state was observed.

Observation of the spectrum in time coincidence with the 1.40-MeV cascade radiation (Fig. 12) established that the 0.353- and 1.12-MeV transitions were in a cascade relationship with the 1.40-MeV transition; the 0.88-, 1.93-, and 2.80-MeV peaks in Fig. 12 correspond to time coincidence involving the 70% contribution to the gating-voltage window from the tails of higher energy spectra. Coincidence measurements on the comparatively weak 1.70-MeV gamma-ray photopeak showed no evidence for any coincident cascading radiations.

The spectrum observed in time coincidence with the 1.93-MeV gamma ray indicated that this transition was in a cascade involving the strong 2.80-MeV as well as the weak 2.45-MeV radiation. The 0.353-MeV radiation

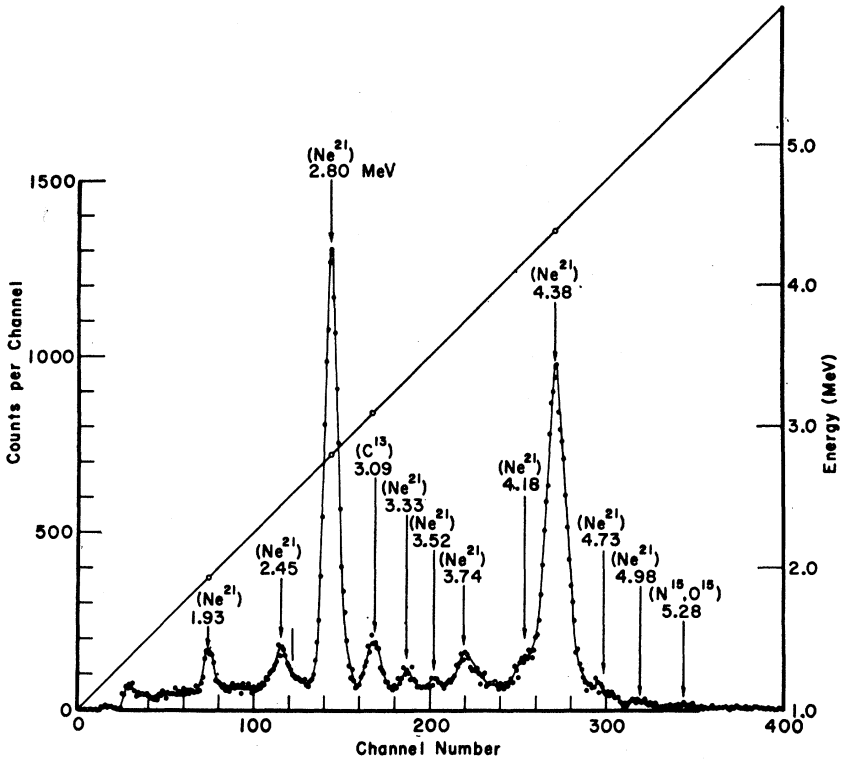

FIG. 13. $Ne^{20}+d$ three-crystal pair-spectrometer spectrum obtained at $\theta=90°$, $E_d=2.20$ MeV.

was also observed in time coincidence here, but a portion of this was introduced by the ~20% contribution of the Compton tails associated with the prominent 4.38-MeV cascade gamma radiation to the coincidence gate channels.

The study of gamma radiations in time coincidence with the prominent 2.80-MeV gamma-ray photopeak confirmed the cascade relationship with the 1.93-MeV radiation, as deduced in the preceding measurement, and also indicated that the 0.88-MeV radiation was in a cascade relationship with the 2.80-MeV transition (Fig. 18). Evidence was also present for the existence of of a 1.63-MeV cascade radiation; this latter transition was not observed in the direct spectrum and consequently was weak, albeit definite, in the coincidence spectrum.

The final coincidence measurement involved radiations in cascade with the intense 4.38-MeV gamma radiation; only the 0.353-MeV gamma ray was observed (Fig. 16).

D. Three-Crystal Pair-Spectrometer Studies

In order to clarify the higher energy portion of the $Ne^{20}+d$ spectra, whose structure was complex in the direct spectra and certain coincidence spectra obtained, the three-crystal pair spectrometer (Fig. 3) was employed. As shown in Fig. 13, the spectrum obtained from this device unambiguously established the presence of 3.33-, 3.52-, 3.74-, and 4.18-MeV gamma-ray transitions in the $Ne^{20}+d$ reactions, and further confirmed the presence of the 1.93-, 2.45-, 2.80-, and 4.38-MeV transitions.

As a check on the higher energy calibrations, a sample of gas analyzing approximately 80% Ne^{20} and 20% $N_2{}^{14}$ was introduced into the target volume. The prominent 5.26- and less intense 5.31-MeV gamma radiations arising from the $N^{14}(d,n)O^{15}$ and $N^{14}(d,p)N^{15}$ [22] were used to obtain an independent check on the standard source calibrations reported herein. Since this calibration was recorded simultaneously with the $Ne^{20}+d$ spectrum, it served as an over-all check on preceding calibration procedures. The energies of the gamma rays associated with the $Ne^{20}+d$ reactions, as determined from this measurement were within the 1% experimental uncertainties of those established by the conventional calibrations of the direct spectrum.

V. TRANSITION ASSIGNMENTS FOR THE GAMMA RAYS FROM $Ne^{20}+d$

A. Gamma Rays from Competing Reactions

There are three reactions which might be expected to introduce impurity gamma radiations in the Ne^{21} spectra obtained at the low bombardment energies

[22] R. D. Bent, T. W. Bonner, J. H. McCrary, and W. A. Ranken, Phys. Rev. **100**, 771 (1955).

employed for these investigations.[23] These are:

(1) $Ne^{20}(d,\alpha\gamma)F^{18}$, $Q_m=+2.78$ MeV;
(2) $Ne^{20}(d,n\gamma)Na^{21}$, $Q_m=+0.22$ MeV;
(3) $Ne^{20}(d,d'\gamma)Ne^{20}$.

Investigations on the gamma-ray de-excitation transitions originating from excited states of the respective residual nuclei in these three reactions have been reported, and their contributions to the study reported herein can be isolated.

(1) $Ne^{20}(d,\alpha\gamma)F^{18}$, $Q_m=+2.78$ MeV

The charged particle spectra following bombardment of neon gas of natural isotopic abundance with 7.8-MeV deuterons has been investigated by Middleton and Tai.[10] The states up to an excitation energy $E_x=4.42$ MeV in F^{18} are bound against alpha-particle emission. It was possible to populate all of the bound states in F^{18} with isotopic spin $T=0$ in the present investigation. Extensive studies of the de-excitation gamma rays in the F^{18} system have been reported by Kuehner, Almqvist, and Bromley.[24] Employing the $O^{16}(He^3,p\gamma)F^{18}$ reaction, these investigators determined the gamma-ray de-excitation scheme for states in F^{18} up to an excitation energy of 3.13 MeV.

No information on the gamma radiations associated with the $Ne^{20}(d,\alpha\gamma)F^{18}$ reaction has previously been reported.[23] When integrated with the information cited above, the results of the investigation reported herein indicated that the integrated total gamma-ray yield for the $Ne^{20}(d,\alpha\gamma)F^{18}$ reaction was at least one order of magnitude less than the corresponding quantity for the $Ne^{20}(d,p\gamma)Ne^{21}$ reaction at deuteron bombardment energies in the 2–3-MeV range.

Evidence for population of the 1.70-MeV ($J^\pi=1^+$, $T=0$) state in F^{18} was found in the coincidence-study results concerning the 1.04-MeV radiation: The 0.66-MeV gamma ray was observed to be in a gamma-gamma cascade with the 1.04 MeV transition. This cascade has been established in F^{18}, involving the 1.70- ($J^\pi=1^+$, $T=0$), the 1.04-MeV ($J^\pi=0^+$, $T=1$), and ground ($J^\pi=1^+$, $T=0$) states. The reported gamma-ray branching ratio for the 1.70-MeV F^{18} state is 69% to the ground state and 31% to the 1.04-MeV state.[24] The branching ratio determined in the present study agreed with this within the limits of the experimental uncertainty if the entire 1.70-MeV gamma-ray photopeak in the $Ne^{20}+d$ spectrum was attributed to the F^{18} transition cited above.

It is further noted that the 1.08-MeV ($J^\pi=(0^-)$, $T=0$) state in F^{18} was probably also populated in this reaction, since the gamma-ray photopeak observed in the 1.04-MeV region of the $Ne^{20}+d$ direct spectra possessed a doublet width and was more intense than the 0.66-MeV photopeak: Direct population of the 1.04-MeV ($T=1$) state via the $Ne^{20}(d,\alpha)F^{18}$ reaction is forbidden by the isotopic selection rule, and hence the formation of this state in this reaction was anticipated to arise solely via cascade transitions from higher lying states. This exhausts the detected contribution of the $Ne^{20}(d,\alpha\gamma)F^{18}$ competing reaction to the $Ne^{20}+d$ gamma-radiation spectrum.

(2) $Ne^{20}(d,n\gamma)Na^{21}$, $Q_m=+0.22$ MeV

Only the lowest lying states in the Na^{21} system are bound levels, corresponding to the ground 0.335-, 1.71-, and 2.43-MeV states; all higher states are unstable against proton emission. The ground-state Q value for this reaction is low relative to that for the $Ne^{20}(d,p)Ne^{21}$ reaction, and it was thus possible to discriminate energetically against formation of the 2.42-MeV Na^{21} state without adversely affecting the formation of high-excitation-energy states in Ne^{21} by an appropriate selection of deuteron bombardment energy. Because of the fact that the 2.45-MeV transition in Ne^{21} was subjected to intensive scrutiny, the energy of the deuteron beam incident upon the nickel window was chosen to be 2.20 MeV for the major portion of the studies reported herein. The mean energy of the 2.20-MeV deuterons after passage through the nickel window was computed[25] and later measured to be 1.83 MeV. At this energy, all of the bound states of Ne^{21} could be formed as regards energetic considerations; the states of excitation energies below 2.05 MeV in Na^{21} could also be formed, but the formation of the 2.42-MeV Na^{21} state was ruled out by the energetics of the reaction. It was possible to form the 0.335- and 1.71-MeV states in Na^{21}, and, because of the proximate excitation energy of the respective mirror nuclear states in Ne^{21} (0.353 and 1.75 MeV), it was not possible to differentiate between transitions from these mirror states by gamma-radiation studies alone. It could be determined that the 0.35- and 1.40-MeV transitions observed in the $Ne^{20}+d$ direct spectrum were overwhelmingly due to the Ne^{20} $(d,p\gamma)$ Ne^{21} reaction by intercomparing the integrated relative cross sections for formation of the Ne^{21} states via the $Ne^{20}(d,p)Ne^{21}$ reaction[12] and the relative gamma-ray intensities detected in the present investigation. It was evident that the $Ne^{20}(d,n\gamma)Na^{21}$ reaction was not a source of severe contamination in the present Ne^{21} studies.

(3) $Ne^{20}(d,d'\gamma)Ne^{20}$

The only excited nuclear state in Ne^{20} which it was energetically possible to populate in the present studies

[23] F. Ajzenberg-Selove and T. Lauritsen, Nucl. Phys. 11, 1 (1959).
[24] J. A. Kuenhner, E. Almqvist, and D. A. Bromley, Phys. Rev. 122, 908 (1961).
[25] J. B. Marion, in *Nuclear Data Tables*, compiled by K. Way *et al.*, (Printing and Publishing Office, National Academy of Science—National Research Council, Washington 25, D. C.), NRC 11-1-11.

TABLE I. Energy levels in Ne^{21} from the $Ne^{20}(d,p)Ne^{21}$ reaction. Λ=Relative integrated capture cross section. $\sigma(90°)$=Relative differential capture cross section at $\theta=90°$. A=Burrows *et al.* (Ref. 12): $E_d=8.5$ MeV; B=Freeman (Ref. 13): $E_d=7.19$ MeV; C=present investigation: $E_d=2.20$ MeV.

State	Excitation energy		l_n	J^π		Λ	$\sigma(90°)$	Decay mode
B	A	B	A	A	C	A	B	C
0	0	0	...		$\frac{3}{2}^+$		0.20	...
1	0.35±0.10	0.349±0.007	2	$\frac{3}{2}^+, \frac{5}{2}^+$	$\frac{5}{2}^+$	1.00	0.39	γ_0
2	1.73±0.10	1.750±0.007	...		$\frac{7}{2}^+$		0.22	γ_0,γ_1
3	2.78±0.05	2.800±0.007	0	$\frac{1}{2}^+$	$\frac{1}{2}^+$	0.53	1.00	γ_0,γ_1
4		2.870±0.007					0.30	γ_2
5		3.666±0.007			$\geq\frac{3}{2}$		0.18	γ_1,γ_3
6		3.737±0.007			$\frac{5}{2}^+$		0.27	γ_0
7		3.889±0.007					0.15	$\gamma_1,(\gamma_0)$
8		4.435±0.007					0.08	γ_3
9	4.58±0.05	4.528±0.007	2	$\frac{3}{2}^+, \frac{5}{2}^+$		0.39	0.43	γ_1
10		4.685±0.009					0.04	
11	4.81±0.05	4.729±0.008	1	$\frac{1}{2}^-, \frac{3}{2}^-$	$\frac{3}{2}^-$	0.76	0.62	$\gamma_1,\gamma_3,(\gamma_0)$
12		5.338±0.008						
13	5.43±0.06	5.434±0.008	2	$\frac{3}{2}^+, \frac{5}{2}^+$				
14		5.550±0.008						
15	5.63±0.06	5.632±0.009	2	$\frac{3}{2}^+, \frac{5}{2}^+$				
16		5.694±0.009						
17	5.78±0.06	5.777±0.009	1	$\frac{1}{2}^-, \frac{3}{2}^-$				
18	5.891.08	5.822±0.009						
19		5.997±0.009						
20		6.036±0.012						
21	6.10±0.08	6.176±0.010						
22		6.267±0.010						
23		6.450±0.012						
24		6.555±0.010						
25		6.606±0.010						
26		6.647±0.012						
27	6.72±0.06	6.748±0.010	2	$\frac{3}{2}^+, \frac{5}{2}^+$				

was the first excited state at 1.63 MeV ($J^\pi=2^+$).[23] No gamma-ray transition corresponding to the de-excitation of this state was observed in the direct spectra reflecting Coulomb-barrier inhibition of this reaction at the energies used here.

B. Gamma Rays from the $Ne^{20}(d,p)Ne^{21}$ Reaction

It has been demonstrated that the transitions observed in the $Ne^{20}+d$ gamma radiation spectrum at $E_d=1.83$ MeV must primarily be associated with the $Ne^{20}(d,p\gamma)Ne^{21}$ reaction. The high ground state Q value of +4.53 MeV for this reaction allowed formation of nuclear states up to an excitation energy of 6.52 MeV in Ne^{21}. The excited states in Ne^{21} are bound ones up to an excitation energy of 6.76 MeV, above which the states are unstable to neutron emission. The nuclear state of highest excitation energy observed to be strongly populated in this study, however, was that at 4.73 MeV.

Pertinent information on the excited states of Ne^{21} determined by Burrows *et al.*[12] and by Freeman[13] is summarized in Table I: The J^π information deduced from the former investigation is presented, as is that determined in the remaining portions of the present research. The gamma-ray decay modes observed for excited states in Ne^{21} via the direct-spectra and time-coincidence measurements previously described herein are also included in Table I. Similar information is illustrated in the energy-level diagram of Ne^{21} (Fig. 26).

VI. ANGULAR CORRELATION STUDIES

A. Angular Distribution Measurements

The angular distributions of the 0.35-, 1.40-, 1.93-, and 4.38-MeV gamma radiations were measured via direct spectral studies with a 5-in.-diam by 4-in.-long sodium iodide crystal (cf. Sec. III) at angles $\theta=0$, 10, 20, 30, 45, 60, 70, 80, 90, and 110° with respect to the beam vector. Similar studies with a 3-in.-diam by 3-in.-long sodium iodide crystal were employed for a second determination of the 0.35-MeV gamma-ray angular distribution; an angular correlation technique was used to provide a second measurement of the 1.93-MeV gamma-radiation angular distribution; and three-crystal pair-spectrometer spectra obtained at angles $\theta=0$, 30, 60, and 90° provided the data for a second determination of the 4.38-MeV gamma-ray angular distribution.

TABLE II. Angular distribution coefficients a_2/a_0.

E (MeV)	a_2/a_0[a]	a_2/a_0[b]	a_2/a_0[c]	a_2/a_0[d]
0.35	−0.04±0.01	−0.07±0.02		
1.40	−0.29±0.03			
1.93	−0.26±0.03		−0.30±0.03	
4.38	−0.01±0.04			−0.02±0.03

[a] Direct spectra in 5 in. ×4 in.
[b] Direct spectra in 3 in. ×3 in.
[c] Angular correlation spectra.
[d] Three-crystal pair-spectrometer spectra.

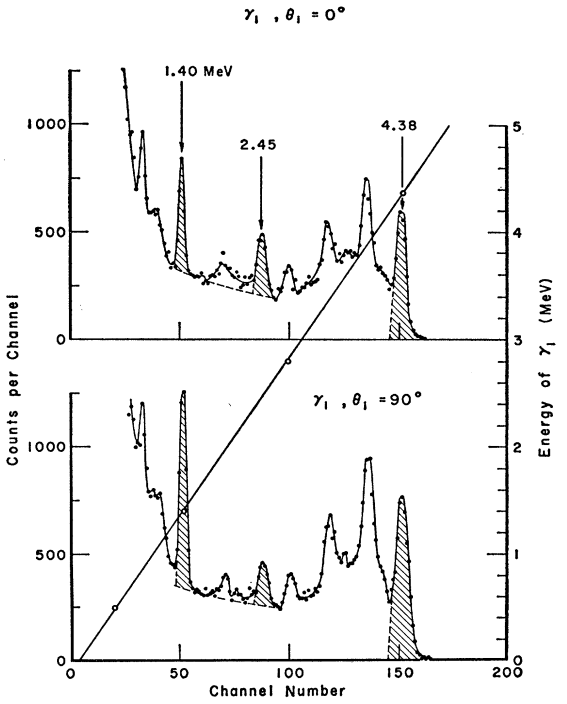

FIG. 14. $Ne^{20}(d,p\gamma_1\gamma_2)Ne^{21}$ gamma-gamma angular correlation spectra for $\theta_2=90°$, $\gamma_2=0.35$ MeV. Upper and lower γ_1 spectra were obtained for $\theta_1=0$ and 90°, respectively. $E_d=2.20$ MeV.

The data thus obtained were fitted by the method of least squares to the equation

$$W(\theta)=1+(a_2/a_0)P_2(\cos\theta)+(a_4/a_0)P_4(\cos\theta). \quad (1)$$

It was determined that inclusion of the $P_4(\cos\theta)$ term did not improve the fit for any of these measurements, $a_4/a_0=0$ within the experimental uncertainty in all cases. The a_2/a_0 coefficients in the above relative intensity distribution function are tabulated (Table II). With the exception of the three-crystal pair-spectrometer measurements, a finite solid-angle correction factor was appropriate for the angular distribution coefficients obtained in these determinations and is included in the tabulated values.

Of particular interest here is the nonzero value of a_2/a_0 for the 1.93-MeV radiation, which the gamma-gamma time-coincidence studies established as arising from the 4.73-MeV state in Ne^{21}. Since the proton angular distribution measurements of Burrows *et al.*[12] affix $J^\pi=\frac{1}{2}^-$ or $\frac{3}{2}^-$ to this state (Table I), the observed anisotropy in this branch of the gamma radiation originating from the 4.73-MeV Ne^{21} state was sufficient to rule out the $J=\frac{1}{2}^-$ possibility: $J^\pi=\frac{3}{2}^-$ for the 4.73-MeV state in Ne^{21}.

B. Angular Correlation Measurements

Six gamma-gamma angular correlation studies were carried out. The two detectors employed were the 3-in.-diam by 3-in.-long sodium iodide crystals, each located 12 cm from the target center (Fig. 2). The procedures outlined previously herein were employed in these measurements, and the incident deuteron beam energy was maintained at 2.20 MeV.

1. $2.80 \xrightarrow{\gamma_1} 0.353 \xrightarrow{\gamma_2} 0$ MeV Ne^{21} Correlation: Case I

Geometry. The time coincidence spectra (depicted in Figs. 11, 13, and 16) indicated that the 2.45-MeV radiation is a cascade transition originating from the 2.80-MeV, $\frac{1}{2}^+$ Ne^{21} state. In order to further substantiate this assignment, the energy of this cascade radiation was re-determined from the three-crystal pair-spectrometer data (Fig. 13), where the peak corresponding to the transition in question was well isolated; the measured energy of this transition at $\theta=90°$ was 2.45 ± 0.01 MeV. A third determination of the transition energy was obtained by simultaneous insertion of a RdTh 2.614-MeV source line in the $Ne^{20}+d$ direct spectrum at $\theta=90°$; the energy of the transition in question was observed to be 2.445 ± 0.015 MeV. Thus, the $2.80 \xrightarrow{\gamma_1} 0.353 \xrightarrow{\gamma_2} 0$ MeV cascade was unambiguously established; in particular, the 2.87 ±0.01-MeV state in Ne^{21} cannot be the initial state in this observed gamma-gamma cascade.

An angular correlation of the radiations in cascade with the 0.353 MeV radiation was subsequently undertaken in Case I geometry[26]: The 0.353-MeV radiation

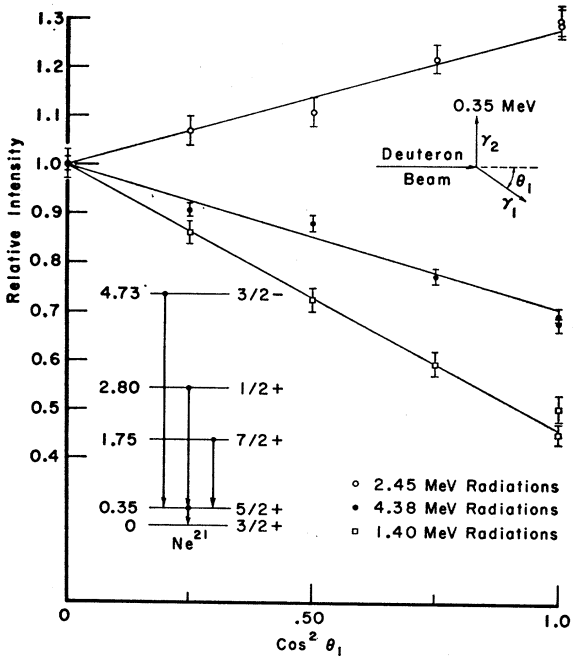

FIG. 15. The angular correlation of the cascade radiations (γ_1) through the 0.353-MeV Ne^{21} state observed in Case I geometry. Relative intensities were computed from the cross-hatched regions exemplified in Fig. 14.

[26] A. E. Litherland and A. J. Ferguson, Can. J. Phys. **39**, 778 (1961).

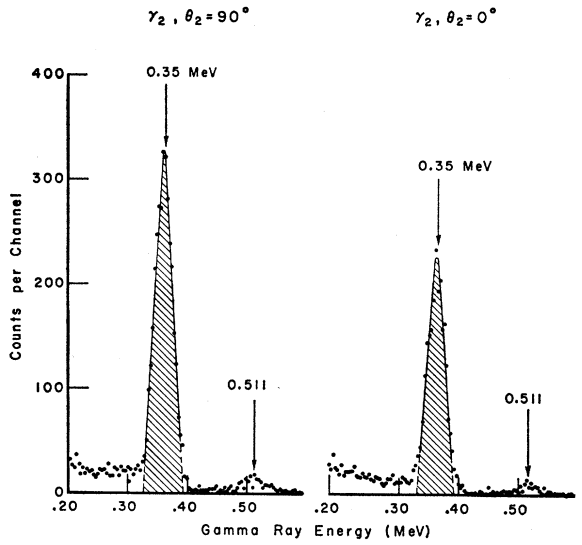

FIG. 16. $Ne^{20}(d,p\gamma_1\gamma_2)Ne^{21}$ gamma-gamma angular correlation spectra for $\theta_1=90°$, $\gamma_1=4.38$ MeV. Left and right γ_2 spectra were obtained for $\theta_2=90$ and 0°, respectively. $E_d=2.20$ MeV.

(γ_2) was observed at an angle θ_2 to the deuteron beam vector, and the 2.45-MeV transition (γ_1) was detected at angles $\theta_1=0$, 30, 45, 60, and 90° to the beam vector, 0 and 90° being repeated.

The angular correlation spectra for $\theta_1=0$ and 90°, respectively, are presented in Fig. 14, where the cross-hatched region at 2.45-MeV energy represents the assumed photopeak area employed for relative intensity comparisons. The experimental correlation is presented in Fig. 15.

The chance coincidence rate was determined to be approximately 20% of the true coincidence rate, and the corrected angular correlation coefficients in Eq. (1) were determined to be $a_2/a_0=-0.19\pm0.02$ and $a_4/a_0=0.02\pm0.02$. Here $\theta=\theta_1+\theta_2=\theta_1+90°$, the angle between the axes of revolution for the two detectors. The geometric correction factors were 15 and 43% for the respective correlation coefficients.[25]

2. $4.73 \xrightarrow{\gamma_1} 0.353 \xrightarrow{\gamma_2} 0$-MeV Ne^{21} Correlation: Case I

Geometry. The measurement of the angular correlation of the cascade radiations participant in the preceding study also provided the data for this correlation (Figs. 14 and 15). The corrected angular correlation coefficient a_2/a_0 was determined to be $+0.25\pm0.03$. As in the preceding study, the higher order coefficient was zero within the limits of the experimental uncertainty.

3. $1.75 \xrightarrow{\gamma_1} 0.353 \xrightarrow{\gamma_2} 0$-MeV Ne^{21} Correlation: Case I

Geometry. This third angular correlation was also obtained from the above experimental studies. Here the appropriate value of a_2/a_0 was determined to be $+0.58\pm0.04$, $a_4/a_0=0$ within the limits of the experimental uncertainty.

4. $4.73 \xrightarrow{\gamma_1} 0.353 \xrightarrow{\gamma_2} 0$ MeV Ne^{21} Correlation: Case II

Geometry. The gamma-gamma cascade radiations involved herein were also amenable to Case II geometry studies,[26] as indicated by the prominence of the 4.38-MeV radiation (γ_1) in the direct spectrum (Fig. 7). The 4.38-MeV radiation was observed at $\theta_1=90°$ with respect to the beam vector, and the 0.353-MeV radiation was detected at the variable angle $\theta_2=0$, 30, 45, 60, and 90°, 0 and 90° being repeated. The angular correlation spectra obtained for $\theta_2=0$ and 90°, respectively, are presented in Fig. 16. The experimental correlations measured in both Case I and II geometries are presented in Fig. 17. The random-coincidence rate was approximately 5% of the real-coincidence rate for Case II angular correlation geometry. The corrected a_2/a_0 term in Eq. (1) was determined to be $+0.33\pm0.02$, and, as in the previously discussed measurements, inclusion of the higher order term in Eq. (1) did not improve the fit.

5. $4.73 \xrightarrow{\gamma_1} 2.80 \xrightarrow{\gamma_2} 0$-MeV Ne^{21} Correlation: Case I

Geometry. The integration of the J^π information now available on the three nuclear states involved in this cascade establishes that this is a $\frac{3}{2}^- \rightarrow \frac{1}{2}^+ \rightarrow \frac{3}{2}^+$ gamma-

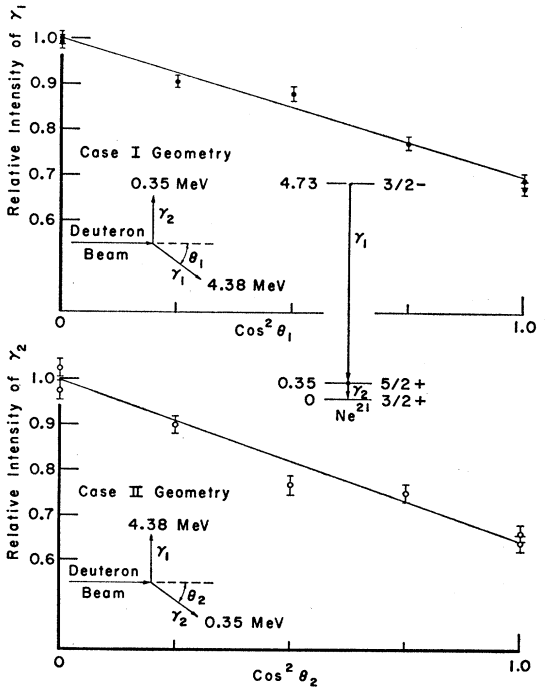

FIG. 17. The angular correlation of the $4.73\gamma_1 \rightarrow 0.353\gamma_2 \rightarrow 0$ MeV cascade radiations in the $Ne^{20}(d,p\gamma_1\gamma_2)Ne^{21}$ reaction. Relative intensities measured in Case I and Case II geometries were computed from the cross-hatched 4.38- and 0.35-MeV photopeak areas exemplified in Figs. 14 and 16, respectively.

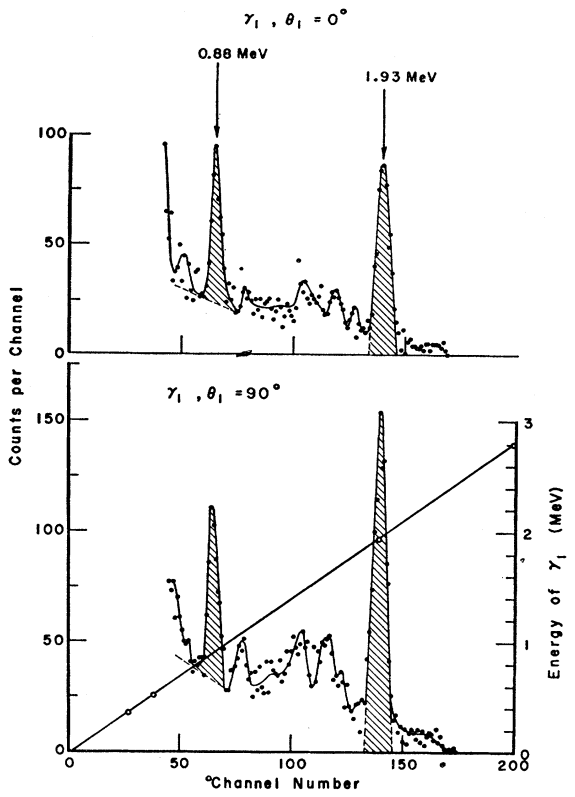

FIG. 18. $Ne^{20}(d,p\gamma_1\gamma_2)Ne^{21}$ gamma-gamma angular correlation spectra for $\theta_2=90°$, $\gamma_2=2.80$ MeV. Upper and lower γ_1 spectra were obtained for $\theta_1=0$ and 90°, respectively. $E_d=2.20$ MeV.

gamma cascade. Since the intermediate state at excitation energy 2.80 MeV possesses spin $\frac{1}{2}$, a measurement of this angular correlation was equivalent to a determination of the angular distribution of γ_1, the 1.93-MeV radiation. Since the latter has been carried out, the former served as a second determination of the angular distribution as well as a check on the correlation procedures and analysis techniques employed herein.

The correlation was measured with γ_2 (the 2.80-MeV radiation) being detected at $\theta_2=90°$, γ_1 being observed at the variable angle $\theta_1=0$, 45, and 90°. The experimental correlation spectra observed at $\theta_1=0$ and 90°, respectively, are presented in Fig. 18. The chance coincidence rate was approximately 20% of the true coincidence rate, and the corrected value of a_2/a_0 in Eq. (1) was determined to be $+0.35\pm0.03$ for this measurement. This corresponds to a value of -0.30 ± 0.03 in a similar expansion for θ_1, and this latter value is in agreement with the value -0.26 ± 0.03 obtained from the direct spectrum angular distribution measurement within the limits of the experimental uncertainty.

6. 3.67 $\xrightarrow{\gamma_1}$ 2.80 $\xrightarrow{\gamma_2}$ 0 MeV Ne^{21} Correlation: Case I

Geometry. The experimental observations just discussed also provided the data for this correlation measurement (Fig. 18). The corrected angular correlation coefficient a_2/a_0 was determined to be $+0.21\pm0.02$, $a_4/a_0=0$ within the limits of the experimental uncertainty. Since the initial transition in this cascade is weak in the direct spectrum and contaminated with the 0.875-MeV O^{17} radiation originating from the entrance window (Fig. 7), no measurement of the angular distribution of γ_1 was obtained in the direct spectral studies. Since this correlation measurement is equivalent to an angular distribution measurement, as noted in the preceding subsection, the nonzero value of a_2/a_0 measured herein is sufficient to eliminate a $J=\frac{1}{2}$ assignment for the 3.67-MeV Ne^{21} state. It can therefore be immediately concluded that $J\geq\frac{3}{2}$ for the 3.67-MeV Ne^{21} state.

VII. INTERPRETATION OF THE ANGULAR CORRELATION MEASUREMENTS

A. Orientation

Since the compound state, or states involved in the (d,p) direct interaction need not have well-defined spin and parity, it is not possible to apply the simple correlation formalism appropriate to resonant reactions or reactions generally which proceed through states of well-defined angular momentum and parity. In consequence, this technique has been relatively little used as yet in stripping studies.

However, at each stage in a multistep cascade correlation, all information regarding the previous reaction steps is represented by a particular orientation of the intermediate state, i.e., by a particular set of unequal magnetic substate populations. In consequence, providing that only the latter stages of the cascade involve well defined states, it is possible to extract meaningful information from the correlation data by including these substate population parameters for the upper state considered among those to be determined from the data in addition to the more usual angular momenta and multipole amplitude ratios. Moreover, under these conditions, the reaction mechanism involved is entirely irrelevant, thus greatly broadening the scope of the correlation techniques. This was first noted by Warburton and Rose[27] and later extended in a more formal and general sense by Litherland and Ferguson.[26] Extensive measurements utilizing this technique on $(p,p\gamma)$ correlation data have recently been reported.

Within the framework of the Litherland-Ferguson formalism the reaction proceeds as follows: A state in the product nucleus of definite spin and parity is formed by a nuclear reaction mechanism (properties unspecified) involving incident and outgoing particles and going through a compound nuclear state of indefinite spin and parity. The quantization axis is defined by the incoming particle, and the outgoing particle is not

[27] E. K. Warburton and H. J. Rose, Phys. Rev. **109**, 1199 (1958).

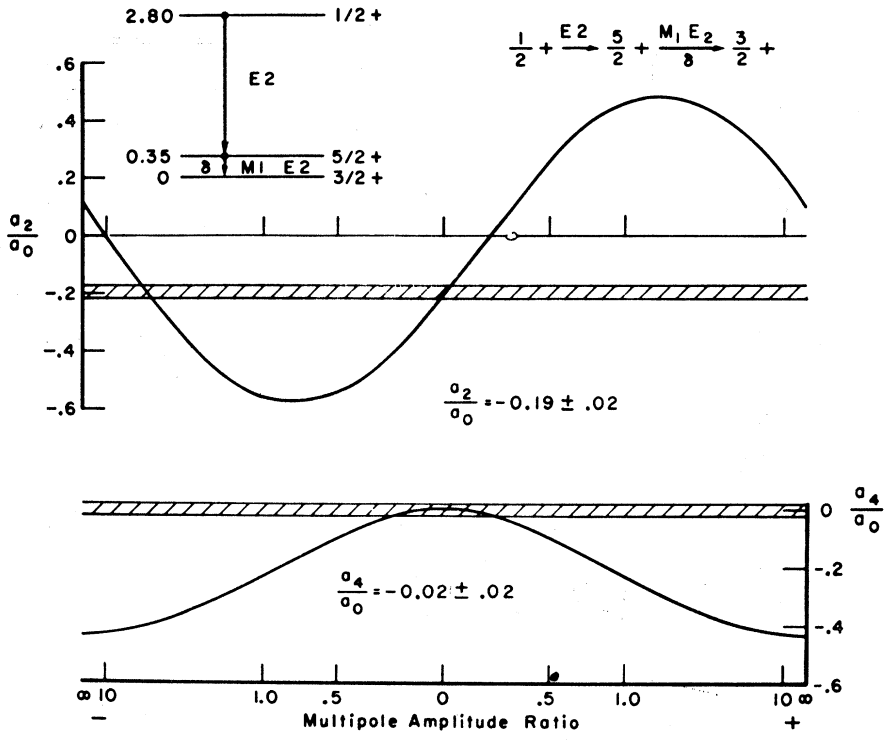

FIG. 19. Gamma-gamma angular correlation coefficients. Cross-hatched regions indicate present experimental determinations discussed in text.

observed. The magnetic substates are uncorrelated and are symmetrically populated (i.e., alignment but not polarization). In such a case, it is possible to express the angular correlation of two successive cascade radiations, γ_1 and γ_2, respectively, in terms of the relative populations of the magnetic substates of the initial (product) nuclear state and the pertinent angular correlation relations presented by Warburton and Rose.[27]

It is important to note that the decay mode for gamma radiation is independent of the magnetic substate populations.[26,28] Thus the population parameters for any state in a multiple cascade are determined solely by the reaction mechanisms in the *formation* of that state. In consequence, the relative populations of the magnetic substates in the product nucleus are identically the same for all gamma-ray transitions originating from this state. In specific situations, sufficient information is available concerning the parameters associated with one gamma decay mode of the product nuclear state so that the population parameters for this state are unambiguously determined. It is then possible to employ these determined values to ascertain information on the characteristics associated with the states and radiations in a *second* or further gamma decay mode originating from this product nuclear state.

Treatment of gamma-gamma angular correlations in cases where either or both of the radiations are of mixed multipolarity is extremely complex when performed in this formalism. In such cases, utilization of the Racah algebra allows recasting of the multiple summations over Clebsch-Gordan coefficients into a more manageable closed form: The development of the pertinent general quadrupole correlation formalism has been presented by Litherland and Ferguson.[26]

[28] D. L. Falkoff and G. E. Uhlenbeck, Phys. Rev. 79, 323 (1950).

B. Applications

1. $2.80 \xrightarrow{\gamma_1} 0.353 \xrightarrow{\gamma_2} 0$ MeV Ne^{21} Correlation

In this case, the initial state in the gamma-gamma cascade is unambiguously a spin-$\frac{1}{2}$ state,[12] and the angular correlation formalism reduces to simple double-cascade theory appropriate to randomly oriented radiations. Treatment of such a case is rendered trivial by

TABLE III. Gamma-gamma angular correlation coefficients: $W(\theta)\sim 1+(a_2/a_0)P_2(\cos\theta)+(a_4/a_0)P_4(\cos\theta)$.

$\frac{1}{2}^+ \xrightarrow[\rho]{M1,E2} \frac{3}{2}^+ \xrightarrow[\delta]{M1,E2} \frac{3}{2}^+$:
$a_2/a_0=\dfrac{(-0.200\pm 0.694\rho+0.775\delta\pm 2.694\rho\delta+0.200\rho^2\pm 0.775\rho^2\delta)}{(1+\rho^2+\delta^2+\rho^2\delta^2)}$
$a_4/a_0=0$
$\frac{1}{2}^+ \xrightarrow{E2} \frac{5}{2}^+ \xrightarrow[\delta]{M1,E2} \frac{3}{2}^+$:
$a_2/a_0=(-0.200\pm 1.015\delta+0.102\delta^2)/(1+\delta^2)$
$a_4/a_0=-0.436\,\delta^2/(1+\delta^2)$

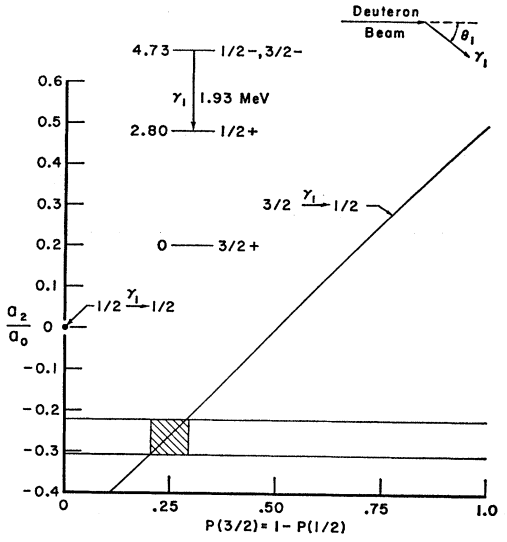

FIG. 20. γ_1 angular distribution coefficients a_2/a_0 as a function of relative magnetic substate populations $P(m_1)$ for pure dipole radiations of $J_1=\frac{1}{2}$ to $J_2=\frac{1}{2}$ and $J_1=\frac{3}{2}$ to $J_2=\frac{1}{2}$ types. Cross-hatched region indicates present experimental determination discussed in text.

the availability of tabulated correlation coefficients.[29] Previous results[12,23] establish that the intermediate state in this cascade possesses spin $\frac{3}{2}$ or $\frac{5}{2}$, the final state has spin $\frac{3}{2}$, and all three states have positive parity. In the event that the intermediate state possessed spin $\frac{3}{2}$, both γ_1 and γ_2 could be mixtures of $M1$ and $E2$ radiations, and the angular correlation coefficients for the $\frac{1}{2}^+(\gamma_1)\frac{3}{2}^+(\gamma_2)\frac{3}{2}^+$ gamma-gamma cascade radiations are presented in Table III. The multipole amplitude ratio $E2/M1$ is expressed as ρ for γ_1 and δ for γ_2, and it is found that the experimentally observed values of the correlation coefficients are consistent with combinations of ρ and δ which allow multipole amplitude ratios in the approximate region -10 to $+10$ for either of the radiations. In the limit $\rho=\delta=0$ (pure dipole transitions), the theoretical a_2/a_0 coefficient is evaluated to be -0.20, the a_4/a_0 coefficient being 0. These values are consistent with the experimentally observed values of -0.19 ± 0.02 and -0.02 ± 0.02, respectively.

In the case that the spin of the intermediate state were $\frac{5}{2}$, γ_1 would be pure $E2$ radiation, and γ_2 would be considered as an $M1$-$E2$ mixture. The theoretical angular correlation coefficients for the $\frac{1}{2}^+(\gamma_1)\frac{5}{2}^+(\gamma_2)\frac{3}{2}^+$ gamma-gamma cascade radiations are also presented in Table III and are presented in graphical form in Fig. 19, where the experimentally observed values of a_2/a_0 and a_4/a_0 are represented by the cross-hatched regions. The measured value of the a_2/a_0 coefficient limits δ, the multipole amplitude ratio for the 0.353-MeV Ne^{21} radiation, to the values $-0.02\leq\delta\leq+0.03$ or $\delta\sim-5$, whereas the observed value of the a_4/a_0 coefficient

[29] D. S. Andreev, K. I. Erokhina, and I. Kh. Lemberg, Izv. Akad. Nauk SSSR Ser. Fiz. 23, 1470 (1959).

TABLE IV. $W(\theta_1)$ and $W(\theta_2)$ angular distribution functions.

J_1	L_1	J_2	$W(\theta_1)$
$\frac{3}{2}$	1	$\frac{1}{2}$	$P(\frac{1}{2})[0.625-0.375\cos^2\theta_1]+P(\frac{3}{2})[0.375+0.375\cos^2\theta_1]$
$\frac{3}{2}$	1	$\frac{3}{2}$	$P(\frac{1}{2})[0.400+0.300\cos^2\theta_1]+P(\frac{3}{2})[0.600-0.300\cos^2\theta_1]$
$\frac{3}{2}$	1	$\frac{5}{2}$	$P(\frac{1}{2})[0.525-0.075\cos^2\theta_1]+P(\frac{3}{2})[0.475+0.075\cos^2\theta_1]$
J_2	L_2	J_3	$W(\theta_2)$
$\frac{3}{2}$	1	$\frac{3}{2}$	$P(\frac{1}{2})[0.480+0.060\cos^2\theta_2]+P(\frac{3}{2})[0.520-0.060\cos^2\theta_2]$
$\frac{5}{2}$	1	$\frac{3}{2}$	$P(\frac{1}{2})[0.570-0.210\cos^2\theta_2]+P(\frac{3}{2})[0.430+0.210\cos^2\theta_2]$

determines that $-0.1\leq\delta\leq+0.1$. Thus, in the case that the intermediate state were spin $\frac{5}{2}$, the multipole amplitude ratio for the final gamma-ray transition would be $-0.02\leq\delta\leq+0.03$, the radiation being pure magnetic dipole within the limits of the experimental uncertainty.

It is concluded that the spin of the intermediate (0.353-MeV Ne^{21}) state is indeterminate in this correlation; either choice of spin is equally acceptable in the analysis, since the respective correlation coefficients for the two cases are identical when pure radiations are present for both cascade transitions. It was therefore mandatory that the spin of the 0.353-MeV Ne^{21} state be determined from other considerations.

2. *Angular Distributions of Radiations from the 4.73-MeV Ne^{21} State*

The pertinent distribution functions[27] for the cascade gamma radiations initiating from unequally populated magnetic substates in the product nucleus were applied to the gamma radiations subsequent to the formation of the 4.73-MeV Ne^{21} state. This state has been shown

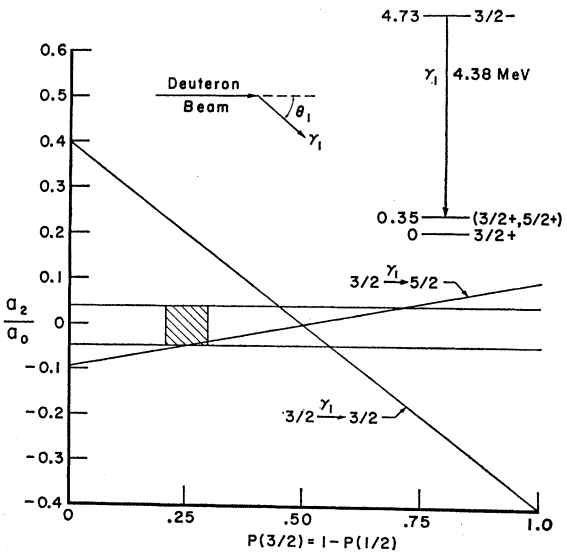

FIG. 21. γ_1 angular distribution coefficients a_2/a_0 as a function of relative magnetic substate populations $P(m_1)$ for pure dipole radiations of $J_1=\frac{3}{2}$ to $J_2=\frac{3}{2}$ and $J_1=\frac{3}{2}$ to $J_2=\frac{5}{2}$ types. Cross-hatched region indicates present experimental determination discussed in text.

TABLE V. Angular correlation function. Define: $W(\theta_1,\pi/2,0)=1+(b_2/b_0)\cos^2\theta_1$; $W(\pi/2,\theta_2,0)=1+(b_2/b_0)\cos^2\theta_2$; $\theta=\theta_1+\theta_2$, $W(\theta)=1+(a_2/a_0)P_2(\cos\theta)$. Then $a_2/a_0=(-b_2/b_0)(\frac{3}{2}+b_2/b_0)^{-1}$.

J_1	L_1	J_2	L_2	J_3	$W(\theta_1,\pi/2,0)$
$\frac{3}{2}$	1	$\frac{3}{2}$	1	$\frac{3}{2}$	$P(\frac{1}{2})[0.431+0.155\cos^2\theta_1]+P(\frac{3}{2})[0.569-0.362\cos^2\theta_1]$
$\frac{3}{2}$	1	$\frac{5}{2}$	1	$\frac{3}{2}$	$P(\frac{1}{2})[0.592-0.158\cos^2\theta_1]+P(\frac{3}{2})[0.408-0.026\cos^2\theta_1]$
					$W(\pi/2,\theta_2,0)$
$\frac{3}{2}$	1	$\frac{3}{2}$	1	$\frac{3}{2}$	$P(\frac{1}{2})[0.431-0.052\cos^2\theta_2]+P(\frac{3}{2})[0.569-0.155\cos^2\theta_2]$
$\frac{3}{2}$	1	$\frac{5}{2}$	1	$\frac{3}{2}$	$P(\frac{1}{2})[0.592-0.276\cos^2\theta_2]+P(\frac{3}{2})[0.408+0.092\cos^2\theta_2]$

herein to possess $J^\pi=\frac{3}{2}^-$, and the 1.93-MeV radiation in the $Ne^{20}+d$ spectrum has been identified as a cascade radiation from the 4.73-MeV $\frac{3}{2}^-$ state to the 2.80-MeV $\frac{1}{2}^+$ state in Ne^{21}. This radiation is therefore essentially pure $E1$ type. The 4.38-MeV radiation has been identified as a cascade radiation from the 4.73-MeV state to the 0.353-MeV state in Ne^{21}; since the latter state possesses either $J^\pi=\frac{3}{2}^+$ or $\frac{5}{2}^+$, this radiation is also anticipated to be essentially pure $E1$ radiation for either spin possibility. Evaluation of the angular distribution functions $W_1(\theta_1)$ [Eq. (1) in Ref. 27] is summarized in Table IV for dipole gamma radiations originating from a spin-$\frac{3}{2}$ state and terminating on spin $\frac{1}{2}$, $\frac{3}{2}$, and $\frac{5}{2}$, respectively. In the evaluation of these angular distribution functions, $P(m_1)=P(-m_1)$ is assumed and the total population of the initial ($J=\frac{3}{2}$) state is normalized to unity by the relation $P(\frac{1}{2})+P(\frac{3}{2})=1$.

The angular distribution of the 1.93-MeV Ne^{21} radiation determined the relative $m_1=\frac{1}{2}$, $\frac{3}{2}$ magnetic substate populations for the 4.73-MeV Ne^{21} state unambiguously. The acute sensitivity of the theoretical a_2/a_0 coefficient for this transition with variation in relative magnetic substate populations was fortuitous; the experimentally observed value $a_2/a_0=-0.27\pm0.04$ restricted $P(\frac{3}{2})$ to the region 0.205 to 0.295, as indicated by the cross-hatched area in Fig. 20. This measurement determined the relative magnetic substate populations for the 4.73-MeV Ne^{21} state as populated in this reaction.

The angular distribution of the second cascade transition originating from the 4.73-MeV Ne^{21} state, which was the 4.38-MeV gamma de-excitation radiation to the $J^\pi=\frac{3}{2}^+$ or $\frac{5}{2}^+$0.353-MeV Ne^{21} state, appeared isotropic within the 4% experimental uncertainty. The cross-hatched area in Fig. 21 represents the graphical region allowed by the relative magnetic substate populations determined from the 1.93-MeV gamma-ray angular distribution measurements discussed above and the experimentally observed angular distribution of the 4.38-MeV radiation. This area included the theoretical a_2/a_0 value in the case that the 0.353-MeV Ne^{21} state possesses spin $\frac{5}{2}$; the theoretical a_2/a_0 coefficient for the alternate spin possibility $\frac{3}{2}$ can be seen to be significantly remote from the experimentally allowed region as depicted in Fig. 21, thus establishing a $\frac{5}{2}^+$ assignment to this state.

3. *Angular Distribution of the Radiations from the 0.353-MeV Ne^{21} State*

Evaluation of the angular distribution function $W_2(\theta_2)$ [Eq. (2) in Ref. 27] is given in Table IV for $J_1L_1J_2L_2J_3=\frac{3}{2}\ 1\ \frac{3}{2}\ 1\ \frac{3}{2}$ and $\frac{3}{2}\ 1\ \frac{5}{2}\ 1\ \frac{3}{2}$, respectively. The relative cross sections for formation of the 0.353- and 4.73-MeV Ne^{21} states by direct particle population via the $Ne^{20}(d,p)Ne^{21}$ reaction are indicated in Table I, and it is evident that the 0.353-MeV Ne^{21} state was formed more than 50% by the direct particle capture mechanism. Since the relative magnetic substate populations from this process were not known, the angular distribution of the 0.353-MeV radiation could not be analyzed unambiguously with the $W_2(\theta_2)$ distribution function. The observed value of $a_2/a_0=-0.07\pm0.02$ for the 0.353-MeV gamma-ray angular distribution was, however, consistent with a $\frac{5}{2}$ spin assignment for this state.

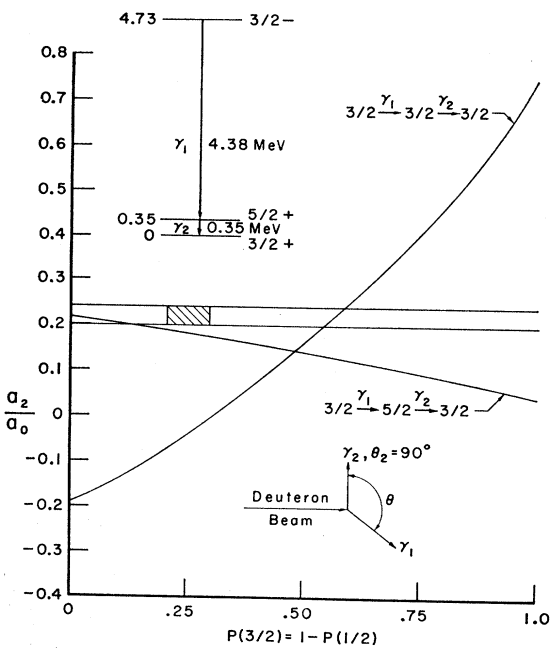

FIG. 22. γ_1-γ_2 angular correlation coefficients a_2/a_0 as a function of relative magnetic substate populations $P(m_1)$ for pure dipole radiations in $J_1=\frac{3}{2}$ to $J_2=\frac{3}{2}$ to $J_3=\frac{3}{2}$ and $J_1=\frac{3}{2}$ to $J_2=\frac{5}{2}$ to $J_3=\frac{3}{2}$ type cascades observed in Case I geometry. Cross-hatched region indicates present experimental determination discussed in text.

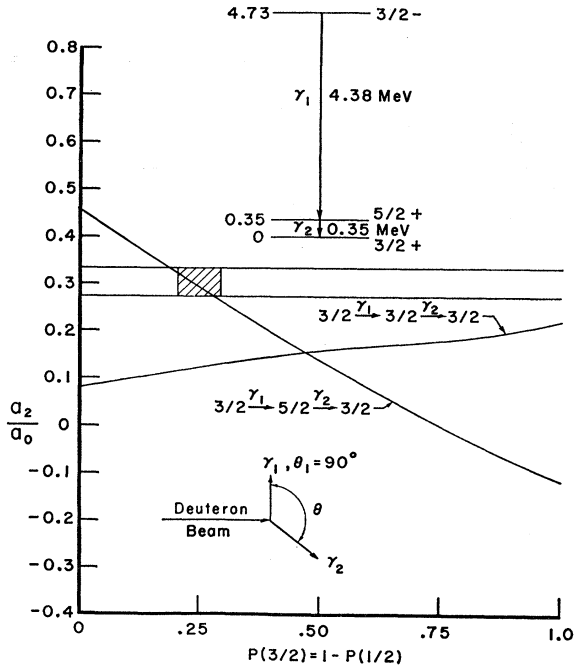

FIG. 23. The angular correlation coefficients described in the caption of Fig. 24 for observations in Case II geometry.

4. $4.73 \xrightarrow{\gamma_1} 0.353 \xrightarrow{\gamma_2} 0$ MeV Ne^{21} Angular Correlations

Further investigation of the spin and multipole mixture assignments indicated by the preceding analyses was possible from this gamma-gamma correlation, which was performed in two geometries. Evaluation of the angular correlation function $W(\theta_1,\theta_2,0)$ [Eq. 3 in Ref. 27] is given in Table V for the $J_1L_1J_2L_2J_3=\frac{3}{2}\ 1\ \frac{3}{2}\ 1\ \frac{3}{2}$ and $\frac{3}{2}\ 1\ \frac{5}{2}\ 1\ \frac{3}{2}$ spin-multipolarity conditions: The $W(\theta_1,\pi/2,0)$ and $W(\pi/2,\theta_2,0)$ functions correspond to the description of angular correlations measured in Case I and Case II geometries, respectively, as demonstrated in Fig. 17. The dipole nature of the cascade radiations ($L_1=L_2=1$) was strongly indicated by the preceding determinations and was assumed for this analysis. For consistency in presentation, the coefficients in Eq. (1), where $\theta=\theta_1+\theta_2$, are obtained by conversion of the tabulated correlation functions to this form (see Table V) and are plotted as a function of the relative magnetic substate populations for the $\frac{3}{2}$—4.73 MeV Ne^{21} state: Figures 22 and 23 indicate the experimental and theoretical a_2/a_0 coefficients for the Case I and Case II correlation geometries, respectively. The cross-hatched areas in these two figures are the experimentally allowed regions, as explained in the prior analyses. The Case I geometry measurement (Fig. 22) illustrates that the theoretical value of the a_2/a_0 coefficient for an assumed intermediate state possessing spin $\frac{5}{2}$ is less than one standard deviation removed from the allowed region, whereas the value corresponding to the $\frac{3}{2}$ alternative case is far removed from it. The results for Case II geometry determination (Fig. 23) indicate that the theoretical value for the a_2/a_0 coefficient for intermediate state spin $\frac{5}{2}$ is included in the experimentally allowed region, whereas that for intermediate spin $\frac{3}{2}$ is significantly remote from the allowed region.

These and the previously discussed measurements unambiguously establish that $J^\pi=\frac{5}{2}+$ for the 0.353-MeV Ne^{21} state. The J^π of the 4.73-MeV Ne^{21} state is further substantiated as $\frac{3}{2}-$. The 0.353-MeV de-excitation radiation is established as predominantly $M1$, the maximum admixture of $E2$ radiation being less than 0.1%.

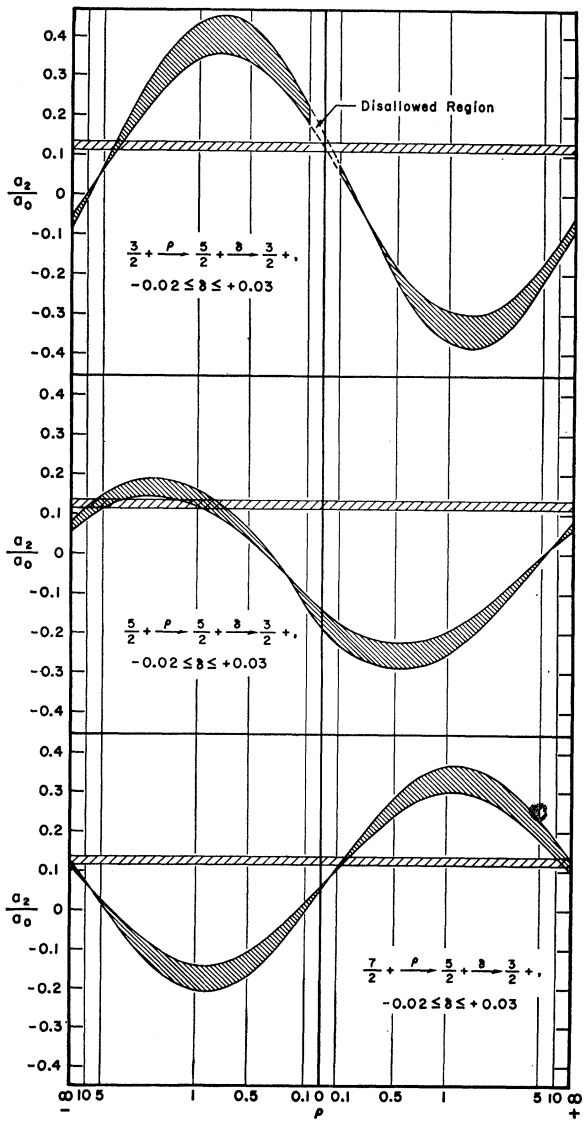

FIG. 24. Gamma-gamma angular correlation coefficients pertinent to the discussion of the two reported angular correlation measurements. Cross-hatched band indicates the region allowed by the determinations reported in Ref. 16, and the broken section in the upper diagram represents region disallowed by the present measurements discussed in the text.

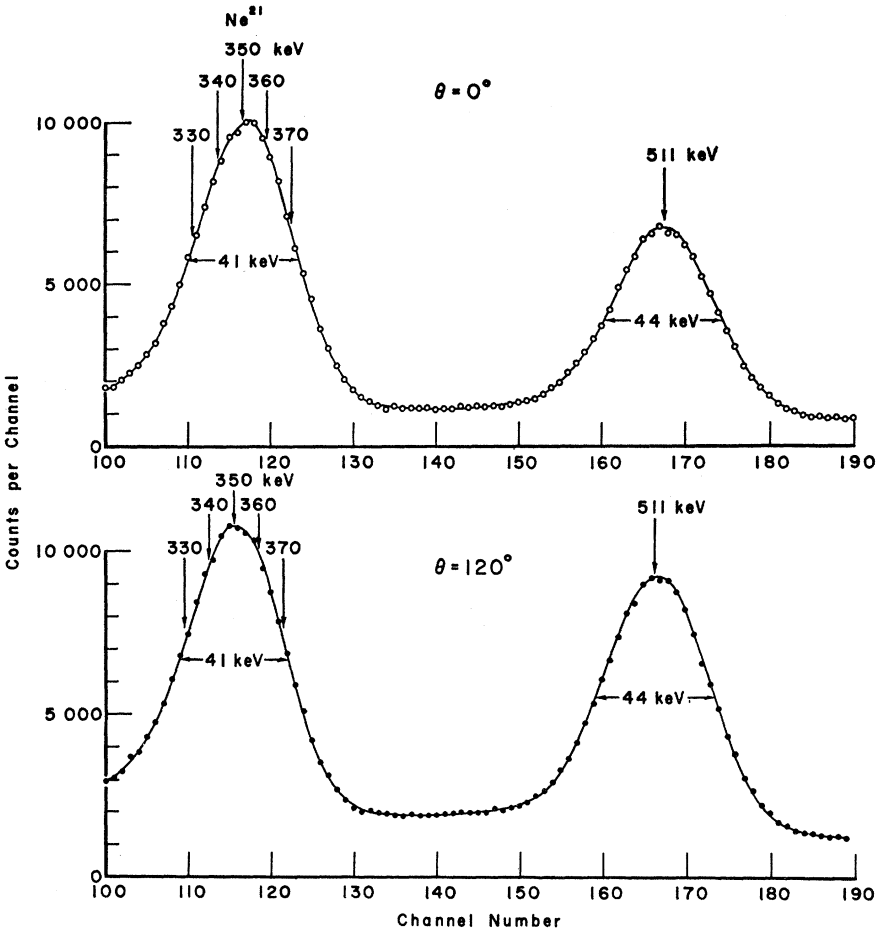

FIG. 25. Spectra illustrating the excitation energy and Doppler-shift measurements for the first excited state of Ne^{21}. Upper and lower spectra were obtained at $\theta=0$ and 120°, respectively. $E_d=2.90$ MeV.

5. $1.75 \xrightarrow{\gamma_1} 0.353 \xrightarrow{\gamma_2} 0$ MeV Ne^{21} Angular Correlation

Since previous studies on the excited states of Ne^{21} have not determined the J^π characteristics for the 1.75-MeV Ne^{21} state,[12,23] only limitations for these static properties can be deduced from the observed de-excitation properties of this state. The particle-gamma time-coincidence measurements established that the 1.75-MeV Ne^{21} decays via branches to both the $\frac{5}{2}^+$ 0.353-MeV and $\frac{3}{2}^+$ 0-MeV Ne^{21} states (Fig. 9), and it is concluded that $\frac{1}{2}\leq J\leq\frac{7}{2}$. The observed anisotropy in the 1.40-MeV gamma-radiation angular distribution (Table II) is sufficient to eliminate the $J=\frac{1}{2}$ possibility.

The measurement of the angular correlation of these same radiations carried out by Khabakhpashev and Tsenter[16] is pertinent to the ensuing analyses. The $O^{18}(\alpha,n\gamma)Ne^{21}$ reaction was studied using a Po-O^{18} combined source-target, and the angular correlation of the radiations involved in the $1.75 \xrightarrow{\gamma_1} 0.353 \xrightarrow{\gamma_2} 0$ MeV Ne^{21} gamma-gamma cascade could therefore be treated within the framework of double-cascade formalism. The angular correlation coefficients associated with the representation in Eq. (1) were determined to be $a_2/a_0=+0.125\pm0.011$ and $a_4/a_0=0$.

Since the J^π values associated with the intermediate and final states as well as the multipole amplitude ratio δ for the second radiation in the cascade are now determined, the values of the multipole amplitude ratio ρ for the first radiation in the cascade that are compatible with the possible J assignments for the initial state can be unambiguously determined. The theoretical angular correlation coefficients are presented in graphical form in Fig. 24 for $J_1=\frac{3}{2}$, $\frac{5}{2}$, and $\frac{7}{2}$, respectively, together with the regions allowed by the determination of Khabakhapshev and Tsenter.

Inspection of Fig. 24 demonstrates that for $J_1=\frac{3}{2}$, $+0.06\leq\rho\leq+0.01$ or $\rho\cong-4$; for $J_1=\frac{5}{2}$, $-0.70\leq\rho\leq-1.2$ or $\rho\cong-5$; for $J_1=\frac{7}{2}$, $+0.17\leq\rho\leq+0.11$ or $\rho\cong\pm\infty$. It is concluded that predominantly dipole character transitions for the 1.40-MeV Ne^{21} de-excitation radiation are compatible only with $J_1=\frac{3}{2}$ or $\frac{7}{2}$. In the event that $J_1=\frac{3}{2}$, the lower allowed region for ρ is seen to be essentially pure dipole ($|\rho|\leq0.04$) in character.

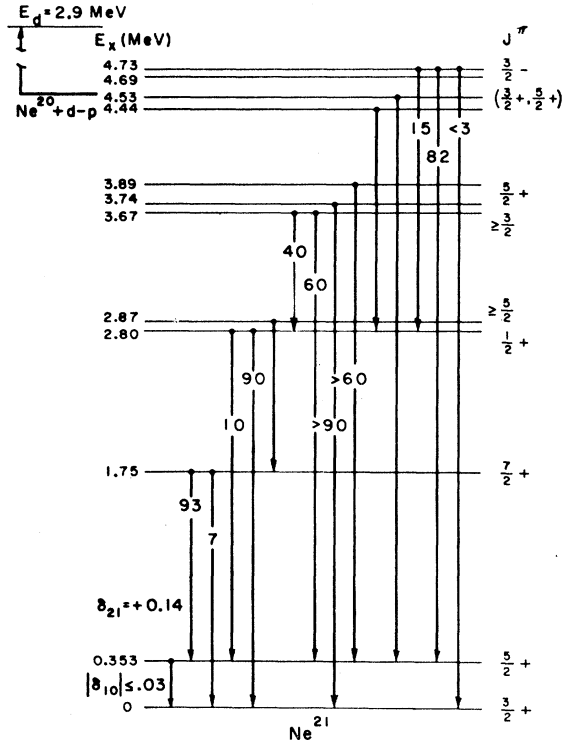

FIG. 26. Energy level diagram for Ne^{21}. Excitation energies are those reported in Ref. 13, spin-parity assignments are those deduced from Ref. 12 and the present work, and the branching ratios are those reported herein.

The angular distribution measurement for the 1.40-MeV radiation and the 1.75-MeV $\xrightarrow{\gamma_1}$ 0.353-MeV $\xrightarrow{\gamma_2}$ 0-MeV Ne^{21} angular correlation in Case I geometry as studied in the present investigation (Table II, Figs. 14 and 15) preclude the latter possibility: No choice of magnetic substate populations $P(\frac{3}{2})$, $P(\frac{1}{2})$ will produce the experimentally observed angular distribution coefficient $a_2/a_0=-0.29\pm0.03$ (Fig. 21) or the experimentally observed angular correlation coefficient $a_2/a_0=0.58\pm0.04$ (Fig. 22) for assumed dipole radiations originating from a $J_1=\frac{3}{2}$ state.

It is thus apparent that a predominantly dipole character transition for the 1.75- to 0.353-MeV Ne^{21} de-excitation radiation is compatible only with $J_1=\frac{7}{2}$, $+0.17\leq\rho\leq+0.11$. Since $J^\pi=\frac{5}{2}+$ for the 0.353-MeV Ne^{21} state, the nonzero value for ρ in this case indicates $\pi=+$ for the 1.75-MeV state.

VIII. LIFETIME AND EXCITATION ENERGY DETERMINATIONS FOR THE 0.353-MeV Ne^{21} STATE

The lifetime of the 0.353-MeV Ne^{21} state has been measured by Khabakhpashev and Tsenter[16]; time-coincidence studies on the gamma radiations emitted from a Po-O^{18} mixture indicated the presence of the gamma-gamma cascade corresponding to the de-excitation of the 1.75-MeV state in Ne^{21} formed by the $O^{18}(\alpha,n_2)Ne^{21}$ reaction, and multichannel time analysis techniques indicated a mean lifetime of $(6.2\pm6.2)\times10^{-11}$ sec for the 0.353-MeV Ne^{21} state.

The partial lifetime of the 0.353-MeV Ne^{21} state against electric quadrupole de-excitation was investigated by Andreev *et al.*[29] via Coulomb-excitation studies. Since J^π for both the ground and 0.353-MeV Ne^{21} states are unambiguously determined, the measurements of Andreev *et al.* determine that the electric-quadrupole partial lifetime of the 0.353-MeV Ne^{21} state is $\tau(E2)=9.2\times10^{-10}$ sec. Comparison of the results of the two studies just discussed indicates predominantly dipole character for the de-excitation radiation from the 0.353-MeV Ne^{21} state, consistent with the angular correlation determinations presented herein.

In the present work, the 0.353-MeV gamma radiation in the $Ne^{20}+d$ spectrum was subjected to Doppler-shift studies: Incident deuterons with energy 2.9 MeV and Ne^{20} gas at an absolute pressure of 50 cm of mercury were employed, 12 spectra being recorded at alternated angles of 0 and 120° with respect to the deuteron beam. The position of the 0.353-MeV gamma radiation was measured relative to the 0.511-MeV annihilation radiation photopeak in each spectrum, as illustrated in Fig. 25, and the energy shift from $\theta=0$ to 120° was determined in this manner to be -2.1 ± 0.4 keV. It was further ascertained from these measurements that the excitation energy for the first excited state in Ne^{21} is 353 ± 1.5 keV.

Kinematical calculations indicated that the mean angle of proton emission consistent with the observed Doppler shift was $75\leq\theta_p\leq85°$ in the laboratory system, and detailed considerations led to the conclusion that this measurement indicated the presence of a full Doppler shift. Using the range and specific energy loss observations reported by Teplova *et al.*,[30] it was determined that the Doppler shift would drop e^{-1} of the full value for $\tau=3\times10^{-10}$ sec. The present investigation imposes a firm limit $\tau<3\times10^{-10}$ sec, consistent with the previously discussed determinations.

IX. BRANCHING RATIO DETERMINATIONS IN THE Ne^{21} SYSTEM

The gamma-ray de-excitation branching ratios for the excited states in Ne^{21} have been extracted from the experimental investigations reported herein. The relative efficiency corrected intensities of the radiations in each of the employed spectra were computed from the area of the gamma-ray photopeaks, which were ascertained by dissection of the total spectra into components by using standard gamma-ray spectral shapes, and were integrated over the range of angles $\theta=0$–90°. These determinations have been summarized in Fig. 26.

[30] Ya. A. Teplova, V. S. Nikolaev, I. S. Dmitriev, and L. N. Fateeva, Zh. Eksperim. i Teor. Fiz. 42, 44 (1962) [English transl.: Soviet Phys.—JETP 15, 31 (1962)].

(*1*) *The 1.75-MeV state.* The direct spectral studies and gamma-gamma time coincidence studies firmly established that the predominant de-excitation mode for the $\frac{7}{2}^+$ 1.75-MeV state is the 1.40-MeV cascade transition to the $\frac{5}{2}^+$ 0.353-MeV state. The gamma radiation observed in the vicinity of 1.75-MeV in the direct spectra (Figs. 6 and 7) was determined to possess an energy of 1.71±0.01 MeV and has been shown to originate from the 1.70-MeV F^{18} state. The proton-gamma time-coincidence measurements (Fig. 9) unambiguously establish the presence of a weak branch to the $\frac{3}{2}^+$ ground state, which accounts for 7±1% of the de-excitation radiations from the 1.75-MeV state.

(*2*) *The 2.80-MeV state.* The principle mode of de-excitation for the $\frac{1}{2}^+$ 2.80-MeV state has been found to be the direct transition to the $\frac{3}{2}^+$ ground state. Positive identification of a weak cascade branch to the $\frac{5}{2}^+$ first excited state has been made, and analysis of the angular distribution spectra (Fig. 6) established that 10.2±0.9% of the de-excitation transitions originating from the 2.80-MeV state is this 2.45-MeV cascade radiation, the remaining percentage being the *M*1-*E*2 direct ground-state transition. Analysis of the 2.45- and 2.80-MeV peaks in the three-crystal pair-spectrometer data (Fig. 13) determined a value of 10.4±1.2% for the relative intensity of the 2.45-MeV cascade branch radiation, and the proton-gamma time-coincidence measurements (Fig. 10) indicated 9.9±1.0% for the relative intensity of this same cascade transition. The various time coincidence measurements reported herein indicated the absence of the previously suggested[15] cascade transition from the $\frac{1}{2}^+$ 2.80-MeV state to the $\frac{7}{2}^+$ 1.75-MeV state.

(*3*) *The 2.87-MeV state.* Inspection of the direct-gamma and three-crystal pair-spectrometer spectra indicated that no significant direct ground-state transition was present for the case of the 2.87-MeV state, for which J^π is unknown. Gamma-gamma time-coincidence measurements determined that the 2.87-MeV state did not detectably de-excite via a direct cascade transition to the $\frac{5}{2}^+$ 0.353-MeV state (Fig. 14), but the 1.13-MeV radiation observed in time coincidence with the 1.40-MeV radiation (Fig. 12) suggested that the 2.87-MeV state decayed via a cascade transition to the $\frac{7}{2}^+$ 1.75-MeV state. Proton-gamma time-coincidence measurements (Fig. 10) verified this assignment. It was concluded that the 2.87-MeV state decays predominantly to the $\frac{7}{2}^+$ 1.75-MeV state.

(*4*) *The 3.67-MeV state.* The direct-spectra and gamma-gamma time-coincidence studies established that the 3.67-MeV state de-excites in part by a 3.33-MeV cascade radiation to the $\frac{5}{2}^+$ 0.353 MeV state. The gamma-gamma time-coincidence studies indicated that this state decays also to the $\frac{1}{2}^+$ 2.80-MeV state via a 0.88-MeV cascade transition (Fig. 18). The three-crystal pair-spectrometer data (Fig. 13) indicated the absence of a direct transition to the $\frac{3}{2}^+$ ground state and established that this latter transition accounted for <10% of the de-excitation transitions from this state. The relative intensities of the 0.88- and 1.93-MeV photopeaks in Fig. 26 were computed, as were those of the 1.93- and 3.33-MeV peaks in Fig. 13. Intercomparison of these results determined that 40±5% of the de-excitations from the 3.67-MeV state proceed to the $\frac{1}{2}^+$ 2.80-MeV state, the remainder decaying to the $\frac{5}{2}^+$ 0.353-MeV state.

TABLE VI. Weisskopf matrix elements for gamma-ray transitions from lower lying states in Ne^{21}.[a]

$E_i \rightarrow E_f$	$\sigma\lambda$	$\lvert M(\sigma\lambda)\rvert^2$
0.353 → 0 MeV	*M*1	>0.005
	*E*2	~45
1.75 → 0 MeV	*M*1	$0.002_{-0.001}{}^{+0.004}$
	*E*2	$5_{-3}{}^{+12}$
1.75 → 0.353 MeV	*M*1	$0.057_{-0.028}{}^{+0.106}$
	*E*2	$210_{-100}{}^{+400}$
2.80 → 0 MeV	*M*1	$0.007_{-0.004}{}^{+0.013}$
	*E*2	$6.5_{-3}{}^{+12}$
2.80 → 0.353 MeV	*E*2	$1.3_{-0.7}{}^{+2.7}$

[a] The mean and/or fractional lifetimes used for the computation of the Weisskopf matrix elements are those from Refs. 16, 18, and 29. The uncertainty in $\lvert M(\sigma\lambda)\rvert^2$ includes the uncertainties in the lifetime and relative gamma-ray intensity measurements.

(*5*) *The 3.74- and 3.89-MeV states.* The three-crystal pair-spectrometer and gamma-gamma time-coincidence data established that the predominant mode of de-excitation for the 3.74-MeV state is the direct transition to the $\frac{3}{2}^+$ ground state, which accounts for >90% of the radiations from the 3.74-MeV state, for which J^π is unknown. These same measurements indicated that the 3.89-MeV state de-excites via a 3.52-MeV cascade transition to $\frac{5}{2}^+$ 0.353-MeV state, greater than 60% of the de-excitation radiations from this state being of this nature.

(*6*) *The 4.44- and 4.53-MeV states.* Spectra observed in time coincidence with the 0.353- and 2.80-MeV gamma-ray transitions (Fig. 14 and 18) established the presence of 4.18- and 1.63-MeV cascade transitions, respectively. The former radiation was also observed in the three-crystal pair-spectrometer spectra, where it was weak compared to and unresolved from the prominent 4.38-MeV peak (Fig. 13). The 4.18-MeV transition is assigned as a cascade radiation from the 4.53-MeV state, for which $J^\pi=(\frac{3}{2}^+,\frac{5}{2}^+)$, to the $\frac{5}{2}^+$ 0.353-MeV state. The 1.63-MeV radiation has been interpreted as a cascade gamma-ray transition from the 4.44-MeV state, for which J^π is unknown, to the $\frac{1}{2}^+$ 2.80-MeV state. No other radiations were detected from these two states.

(*7*) *The 4.69- and 4.73-MeV states.* The 4.69-MeV state is very weakly populated compared to the $\frac{3}{2}^-$ 4.73-MeV state by particle-capture mechanisms (Table I). No radiations were detected from the former state, for which J^π is unknown, whereas positive identification of two cascade radiations originating from the 4.73-MeV state has been made by gamma-gamma time-coincidence measurements (Figs. 14, 16, and 18). Analysis of the

angular distribution spectra indicated that of the total transitions from the 4.73-MeV state, $14\pm1\%$ was the 1.93-MeV transition to the $\frac{1}{2}^+$ 2.80-MeV state, $83\pm1\%$ was the 4.38-MeV radiation to the $\frac{5}{2}^+$ 0.353-MeV state, and less than 3% was the direct de-excitation to the $\frac{3}{2}^+$ ground state. The corresponding percentages obtained from the three-crystal pair-spectrometer data were $15\pm1\%$, $82\pm1\%$, and $<3\%$, respectively.

X. SUMMARY OF SPECTROSCOPIC DATA

In this section, the results reported herein are integrated with presently available data to establish spectroscopic characteristics of several of the Ne^{21} states under discussion. Combining relevant lifetime and branching ratio determinations, the single-particle matrix elements have been computed for possible transitions originating from the lower lying states in Ne^{21} and are presented in Table VI.

(*1*) *The ground state.* The atomic beam measurements of Grosof *et al.*[31,32] have determined $J=\frac{3}{2}$ for the Ne^{21} ground state. When combined with the established positive parity of the first excited state of Ne^{21}, the Coulomb excitation measurement of Andreev *et al.*[29] indicates like parity for the Ne^{21} ground state. This also accords with the observed branching ratios for the $\frac{7}{2}^+$ 1.75- and $\frac{1}{2}^+$ 2.80-MeV states (Fig. 26) and the single particle matrix elements for transitions from these states (Table VI).

(*2*) *The 0.353-MeV state.* The $J^\pi=\frac{5}{2}^+$ assignment to the first-excited state of Ne^{21} is unambiguously established from the $l_n=2$ character of the pertinent proton angular distribution in the $Ne^{20}(d,p)Ne^{21}$ reaction[12] and the angular correlation measurements presented herein (Sec. VII).

(*3*) *The 1.75-MeV state.* In order to reduce the apparent enhancement of the $E2$ component of the $1.75\rightarrow0.353$ MeV transition shown in Table VI to a value consistent with either systematic data and such enhancement in the *sd* shell or with crude estimates of the upper limit for such enhancements obtained by coherent summation of contributions from all protons in the nucleus,[33] it must be concluded that a multipole amplitude ratio $|\rho|\lesssim0.4$ is involved in the actual transition. As illustrated in Fig. 24 and discussed in Sec. VII, the only J^π assignment for which $|\rho|\leq0.4$ is $J^\pi=\frac{7}{2}^+$. This assignment is consistent with the observed $|M(E2)|^2\sim5$ value for the direct ground-state de-excitation of the 1.75-MeV state. This J^π determination is also confirmed by Pelte *et al.* from $F^{19}(He^3,p\gamma)Ne^{21}$ studies,[17] as is the multipole amplitude ratio for the $1.75\rightarrow0.353$ MeV transition, $+0.11\leq\rho\leq+0.17$, deduced herein.

(*4*) *The 2.80-MeV state.* The present studies confirm the $J^\pi=\frac{1}{2}^+$ nature of the 2.80-MeV state established by Burrows *et al.* from the $l_n=0$ behavior of the associated proton group angular distribution.[12] The branching ratio for this state as determined herein is in marked disagreement with that deduced by Pelte *et al.* from $F^{19}(He^3,p\gamma)Ne^{21}$ studies.[17] Should this discrepancy be substantiated by further measurements, the only apparent explanation involves postulation of an as yet unresolved doublet at this excitation energy whose members are preferentially populated in the $(d,p\gamma)$ and $(He^3,p\gamma)$ reactions, respectively.

(*5*) *The 2.87-MeV state.* Since the predominant de-excitation of this state is via a cascade transition to the $\frac{7}{2}^+$ 1.75 MeV state, a $J\geq\frac{5}{2}$ limitation is indicated.

(*6*) *The 3.67-MeV state.* The anisotropy in the 0.88-MeV cascade radiation to the 2.80-MeV Ne^{21} state (Sec. VI) establishes $J\geq\frac{3}{2}$. Combining this limitation with that of Pelte *et al.*,[17] namely $J=\frac{1}{2}$ or $\frac{3}{2}$, a unique assignment of $J=\frac{3}{2}$ is determined; however, the parity is as yet undetermined.

(*7*) *The 3.74-MeV state.* Morpurgo[34] has investigated the factors pertinent to the gamma de-excitation properties of mirror nuclear states in the light mass region of the nuclides and has demonstrated that the invariance of internucleon forces with respect to charge symmetry has important consequences for the relative strengths of corresponding dipole transitions in mirror nuclear systems. Taking into consideration Coulomb and exchange interactions, the strengths of corresponding magnetic dipole transitions should not in general differ by more than a factor of 1.5 when normalized energetically.

Our investigation of the 1170-keV resonance in the $Ne^{20}(p,\gamma)Na^{21}$ reaction has established $J^\pi=\frac{5}{2}^+$ for the 3.57-MeV Na^{21} state[1,2]; this state is observed to decay to decay by predominantly magnetic dipole radiation 85, 4, and 11% to the ground, first, and second excited states of Na^{21}, respectively.

The energy corrected ratio of magnetic dipole transition strengths ($\eta_{f,f'}{}^c$ in Morpurgo's notation[34]) observed for the branches from the 3.57-MeV Na^{21} state to the first-excited and ground states, respectively, in Na^{21} is 0.06. The corresponding ratios applicable to the 3.74- and 3.89-MeV Ne^{21} states are $\lesssim0.2$ and $\gtrsim2.0$, respectively.

Although there is insufficient information presently available to establish a J^π assignment for the 3.74-MeV Ne^{21} state directly, an intercomparison of the energy spectra of, and the appropriate Morpurgo ratios given above for, the Ne^{21}–Na^{21} mirror nuclear systems indicates that the 3.74-MeV Ne^{21} and 3.57-MeV Na^{21} states are almost certainly mirror analog levels with $J^\pi=\frac{5}{2}^+$.

(*8*) *The 4.73-MeV state.* In conjunction with the measurements of Burrows *et al.*[12] and of Freeman[13] on

[31] G. M. Grosof, P. Buck, W. Lichten, and I. I. Rabi, Phys. Rev. Letters **1**, 214 (1958).
[32] J. C. Hubbs and G. M. Grosof, Phys. Rev. **104**, 715 (1956).
[33] D. H. Wilkinson, in *Nuclear Spectroscopy*, edited by F. Ajzenberg-Selove (Academic Press Inc., New York 1960), Chap. V. F.
[34] G. Morpurgo, Phys. Rev. **114**, 1075 (1959).

the $Ne^{20}(d,p)Ne^{21}$ reaction, the present studies establish $J^\pi=\frac{3}{2}^-$ for this level.

XI. ASPECTS OF COLLECTIVE BEHAVIOR

A. Odd-Nucleon Count $\zeta=11$ Systems

Strong-coupling collective models have enjoyed very considerable success in correlating available experimental data on even-even nuclei such as Mg^{24} and Ne^{20} near the beginning of the *sd* shell, and in particular those on the $\zeta=13$, odd-mass mirror pair Mg^{25} and Al^{25}. Relatively less consideration has been devoted to the $\zeta=11$ systems (i.e., O^{19}, Ne^{21}, Na^{21}, and Na^{23}), reflecting the paucity of relevant experimental data.

With the availability of the results presented herein, it becomes of considerable interest to examine the applicability of the many variants of the strong-coupling model now in use and in addition to attempt to adduce evidence favoring one of these.

Assuming, on the basis of the experimentally observed positive quadrupole moment, and other evidence from neighboring nuclei bracketing the $\zeta=11$ systems, that these latter nuclei have static prolate core deformations ($\eta>0$), it follows that the odd nucleon in each case would be expected to occupy Nilsson orbit 7 with $\Omega^\pi=\frac{3}{2}^+$, in the ground-state configurations, and that any rotational structure based on this and higher intrinsic states would be expected to be essentially identical in all the $\zeta=11$ nuclei. The experimentally determined level spectra in these $\zeta=11$ systems support this expectation.

The experimental data presented herein on the Ne^{21} level spectrum strongly suggests identification of $K^\pi=\frac{3}{2}^+$ ground-state rotational band, consistent with the above assumption. Examination of the Nilsson diagram suggests the presence of excited intrinsic configurations having $K^\pi=\frac{1}{2}^+$ and $\frac{5}{2}^+$ corresponding to odd-nucleon promotion to orbits 9 and 5 based, respectively, on $s_{1/2}$ and $d_{5/2}$ spherical shell-model states.

The 2.80-MeV Ne^{21} state has been demonstrated to have a $\frac{1}{2}^+$ assignment and has previously been suggested as the $K^\pi=\frac{1}{2}^+$ band head; no equivalently unambiguous candidate has yet been identified as the $K^\pi=\frac{5}{2}^+$ band head.

In the $\zeta=13$ system, where rotational phenomena have been most clearly evident in this mass region, three of the lowest lying rotational bands have $K^\pi=\frac{5}{2}^+$, $\frac{1}{2}^+$ and $\frac{1}{2}^-$; as such their intrinsic wave functions are not mixed in first order by the dominant Coriolis perturbation, consistent with the experimental observations. In the $\zeta=11$ systems, on the other hand, the possible presence of overlapping $K^\pi=\frac{3}{2}^+$, $\frac{1}{2}^+$ and $\frac{5}{2}^+$ bands implies strong $\Delta K=1$ Coriolis mixing of the state wave functions with consequent obscuration of simple rotational phenomena. It is thus not surprising that only qualitative evidence for such strong coupling behavior has been adduced from the $\zeta=11$ data. In the following sections we consider, separately, the available information on the low lying positive and negative parity states.

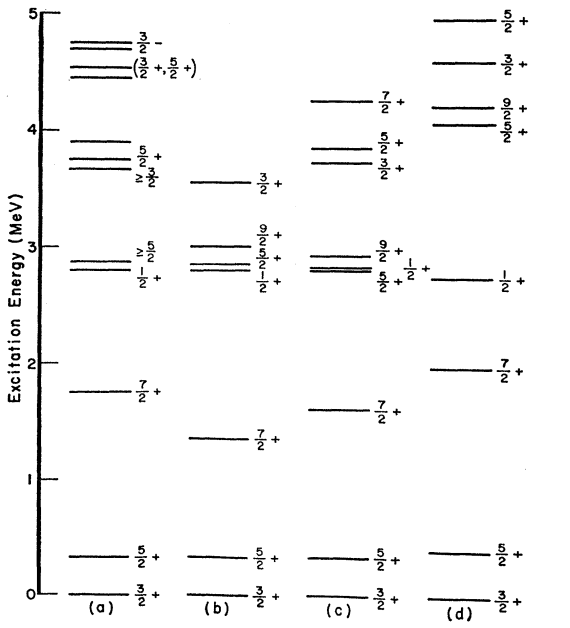

FIG. 27. Comparison of the experimentally observed energy spectrum of Ne^{21} (a), with those generated by the collective model calculations in Refs. 7, 8, and 4b, c, and d, respectively).

B. Positive-Parity States

On the basis of the static properties of Ne^{21}, including the above mentioned level spectrum, the ground-state electric quadrupole moment $Q=0.093+0.010$ b,[31] and the ground-state magnetic moment $\mu=-0.662$ nm,[32] comparison with the Nilsson calculations suggests a deformation $3\leq\eta\leq4$ as appropriate to the description of this nucleus. This is in accord with the equivalent parameter choice for Na^{21} and Na^{23}.

Invoking Coriolis mixing of the three Nilsson bands already noted, Freeman[7] has extended the earlier Paul-Montaque treatment of Na^{23} to the Ne^{21} system. Dreizler,[8] in a similar calculation, coupling an *sd* neutron to a prolate Ne^{20} core, has predicted static and dynamic properties of the Ne^{21} levels to an excitation of about 6 MeV. Chi and Davidson[4] have evolved an asymmetric rotor model applicable to *sd* nuclei and have suggested that a best fit to the experimental data, with a minimum number of theoretical parameters, requires a strongly asymmetric-core deformation characterized by $\gamma\sim20°$. Roesser and Davidson[35] have more recently attempted to improve the agreement between this latter model and the experimental data by incorporating a beta-vibrational term in the Hamiltonian;

[35] J. Roesser, Doctoral dissertation, Rensselaer Polytechnic Institute 1964 (unpublished).

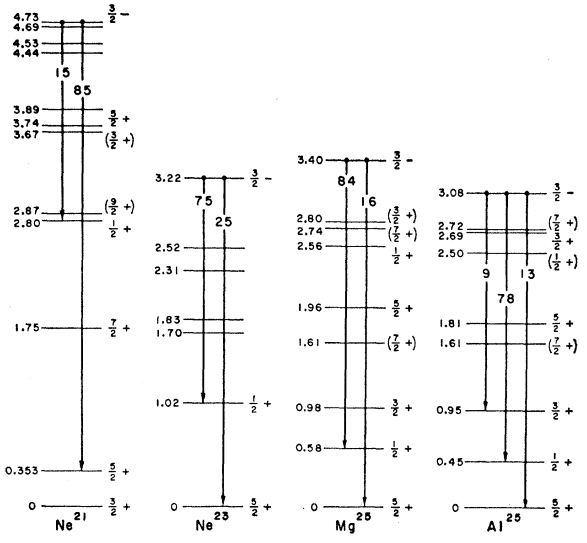

FIG. 28. Intercomparison of the properties of the lowest lying $J^\pi=\frac{3}{2}^-$ states presently identified in the adjacent odd-A nuclear systems Ne^{21}, Ne^{23}, Mg^{25}, and Al^{25}.

the corresponding gamma-vibrational terms were neglected in the light of results in the rare-earth region of strong deformation, where such neglect has been demonstrated to be entirely justified.[36] This lastest model again suggests an asymmetric-core shape with $\gamma\sim 20°$ but does not provide significant improvement in the agreement with experiment.

Figure 27 compares the results of the first three of the above model calculations with the experimental spectrum.

It is immediately apparent from this figure that no unambiguous conclusions may be drawn regarding relative merits of these calculations pending the availability of considerably more extensive spectroscopic assignments to higher excited states. Such work is currently in progress in this and other laboratories.[18,37]

While the model states generated by Freeman[7] and Dreizler[8] appear to provide a more adequate representation of the data than do those of Chi and Davisson,[4] it must be emphasized that the number of model parameters is significantly less in the latter case.

A similar situation holds regarding the dynamic properties of these low-lying states. As discussed previously, although absolute transition strengths have not been measured, the branching ratios measured in the de-excitation of the Ne^{21} states at 1.75 and 2.80 MeV (see Figs. 19 and 26) are consistent with enhancement of the $E2$ widths, inhibition of the $M1$ widths, or both. The spheroidal Nilsson model predictions, incorporating Coriolis band mixing, are in reasonable accord[6,17] with the observed branching ratio for the 1.75-MeV state, as is also the case in Na^{23} for the de-excitation branching from the $\frac{7}{2}^+$ 2.08-MeV state. For these same transitions, the asymmetric rotor model predictions are characteristically incorrect by at least two orders of magnitude, reflecting much smaller enhancement or inhibition of the $E2$ transitions as compared to the equivalent symmetric-model predictions.

In the de-excitation of the 2.80-MeV state, the observed branching ratio suggests that intra- and inter-band $E2$ transition enhancements in Ne^{21} are of the same order. While this in general might be attributed to strong Coriolis mixing of the band members so that the distinction between bands is essentially lost, in the present instance the $\frac{1}{2}^+$ 2.80-MeV state would be expected to be pure $K=\frac{1}{2}^+$ since no corresponding J^π state is available for mixing in the overlapping $K^\pi=\frac{3}{2}^+$ and $\frac{5}{2}^+$ bands. The amount of $K^\pi=\frac{1}{2}^+$ mixing in the $K^\pi=\frac{3}{2}^+$ ground state required to fit the static properties is much too small to provide the observed enhancement. In this case, the asymmetric rotor model calculations are again not significantly different from the extreme single-particle Weisskopf estimates and are also in disagreement with observations.

It would clearly be premature to attempt to draw any conclusions regarding relative applicability of these strong-coupling models from these data, particularly in view of the smaller number of parameters incorporated in the Chi-Davidson asymmetric rotor model.

The qualitative success of these models generally, however, makes very probable J, π, K assignments of $\frac{9}{2}$, $+$, $\frac{3}{2}$ and $\frac{3}{2}$, $+$, $\frac{1}{2}$, respectively, to the Ne^{21} states at 2.87 and 3.67 MeV excitation.

C. Negative-Parity States

Although as yet, only isolated negative-parity states have been identified in odd-A *sd* shell nuclei, these are of particular interest in establishing the validity of the strong-coupling models which make specific predictions regarding their occurrence either as hole states or as predominantly single-particle excitations to negative parity orbits, i.e., those based on the $f\frac{9}{2}$ configuration. In prolate spheroidal nuclei the $\Omega^\pi=\frac{1}{2}^-$ state drops rapidly in energy with increasing deformation and would be expected to be relatively isolated as the lowest negative-parity state. In ellipsoidal nuclei ($\gamma\neq 0$), it has been shown that a number of negative parity states drop together in energy with increasing γ.

Evidence has recently been obtained for the systematic occurrence of a $\frac{3}{2}^-$ state in odd-A nuclei in this mass region[38] which might *a priori* be taken as evidence for $\gamma\neq 0$.

Examples are the following: Ne^{21}(4.73 MeV), Ne^{23}(3.22 MeV), Mg^{25}(3.40 MeV), and probably

[36] J. S. Greenberg, G. G. Seaman, E. V. Bishop, and D. A. Bromley, Phys. Rev. Letters **11**, 211 (1963).

[37] H. T. Motz, and E. T. Jurney, Bull. Am. Phys. Soc. **8**, 335 (1963).

[38] A. J. Howard and D. A. Bromley, Bull. Am. Phys. Soc. **9**, 439 (1964).

Mg^{27}(3.56 MeV). It must be noted, however, that these same states are very strongly and selectively populated by (d,p) stripping reactions, even at energies at and below the relevant Coulomb barriers, suggesting a dominant single particle amplitude in the state wave function. Preliminary calculations suggest that such a state may have a significantly mixed pf configuration.[39]

Various attempts have been made previously to fit these negative-parity states into a Nilsson-model description. In Mg^{25}, the 3.40-MeV state has been taken as a member of the $K^\pi=\frac{1}{2}^-$ band based on orbit 14 with $\Omega^\pi=\frac{1}{2}^-$. As noted previously, the predicted energy of this state varies rapidly with deformation and thus may provide a sensitive determination of the equilibrium shape.

While it would be tempting to attribute the negative-parity state at 5.77 MeV[12,13] in Ne^{21} as the $J=\frac{1}{2}$ member of a rotational band based on the $\frac{3}{2}^-$ state at 4.73 MeV, no adequate evidence exists for such an assignment as yet. As indicated in Fig. 28, the inhibition of the $E1$ de-excitation of the 3.22-MeV state in Ne^{23} may be attributed to the applicable K selection rule, since $\Delta K=2$ for this transition, analogous to those in the Al^{25} and Mg^{25} members of the $\zeta=13$ system. The apparent inhibition factors in the three cases are ~ 5, providing a measure of the model validity in these totally model forbidden transitions.

In the de-excitation of the Ne^{21} 4.73-MeV state, transitions to the $\frac{1}{2}^+$ and $\frac{5}{2}^+$ states at 2.80 and 0.353 MeV, respectively, and to the $\frac{3}{2}^+$ ground state are all K allowed. The branching ratios measured suggest that the ground-state transition is inhibited by a factor of roughly 50 relative to the others; this inhibition is not predicted by the Nilsson model or its mixed variants already referred to nor by the asymmetric rotor models.

[39] B. R. Mottelson (private communication).

It is clear from the remarks of this section that even in this heavily studied region of the *sd* shell, it is not yet possible to draw any unambiguous conclusions regarding equilibrium nuclear shapes or the relative merits of different formulations of the strong-coupling collective models, although qualitative successes thus far attained strongly support the validity of this general approach. As in the case of the nuclear optical model, evolution of adequate fits to experimental data through proliferation of model parameters must be guarded against, and in this respect the work of Davidson and co-workers and of Kelson and Levinson[40] is particularly interesting.

Much more experimental data is badly needed in this mass region where extensive calculations are becoming available. We are currently making further measurements on O^{19}, Ne^{23}, and Na^{23} to provide such data[38,41] and are calculating moments and transition probabilities in this region within the framework of the Kelson-Levinson model. These results will be reported in a later paper, which will include a detailed analysis of all the available data on the $\zeta=11$ systems.

ACKNOWLEDGMENTS

We wish to thank Professor W. W. Watson for his contribution in the production of the monoisotopic target material used in the experimental investigations. We also thank the technical staff of the Brookhaven National Laboratory Van de Graaff accelerator, in particular R. A. Lindgren, for their assistance during the experimental investigations. We are indebted to Dr. D. E. Alburger for his hospitality at the Brookhaven National Laboratory and his interest and encouragement during the course of these measurements.

[40] I. Kelson and C. Levinson, Phys. Rev. **134**, 2189 (1964).
[41] A. J. Howard, J. P. Allen, D. A. Bromley, and J. W. Olness, Bull. Am. Phys. Soc. **9**, 68 (1964).